POLITECNICO DI TORINO

Corso di Laurea in Ingegneria Biomedica

Tesi di Laurea Magistrale

Applications of Source Detection in Biomedical Signals

Relatore
Prof. Luca Mesin

Candidato
Stefano Rivera

Contents

Abstract 3

1 Blind Source Separation 4
- 1.1 Introduction . . . 4
- 1.2 Methods . . . 5
  - 1.2.1 Principal Component Analysis . . . 7
  - 1.2.2 Independent Component Analysis . . . 10

2 Inverse Problem in Electroencephalography 15
- 2.1 Neurophysiologic introduction of the EEG . . . 15
- 2.2 EEG Inverse Problem . . . 16
  - 2.2.1 Mathematical Formulation . . . 18
  - 2.2.2 Equivalent Current Dipoles . . . 19
  - 2.2.3 Distributed Source Models . . . 20

3 EMG Decomposition 23
- 3.1 The Surface Electromyogram . . . 23
- 3.2 Separation of Single Muscles . . . 25
- 3.3 Separation of Motor Unit Action Potentials . . . 28
  - 3.3.1 Data Model . . . 28
  - 3.3.2 Convolution Kernel Compensation . . . 30
  - 3.3.3 ICA Decomposition . . . 31

4 An Alternative Method for Crosstalk Reduction 37
- 4.1 The Problem of Crosstalk . . . 37
- 4.2 Optimal Spatio-Temporal Filter . . . 38
  - 4.2.1 Experimental Signals . . . 39

APPENDIX 44

References 48

Abstract

The detection of the sources is a mathematical problem that can find application in all that fields in which a mixture of different signals is available: it is widely used in acoustics [16], where different sounds can be received by multiple microphones, in decoding communication signals taken by antennas [4], in separation of seismic data [20] and in image processing [18], just to name a few.

In biomedical signal processing, the source detection can help in decoding the complex brain activity from electroencephalographic (EEG) data, in studying muscle activation from electromyographic (EMG) recordings and also finds some interesting applications in electrocardiography (ECG), where maternal and foetal ECG were considered as two distinct sources and thus were separated [24].

The term blind source separation (BSS) arises from the fact that the solution is recovered with a blindly approach: limited or no a priori information is assumed on the sources and on the propagating medium in which the signals travel to reach the receiver. With this approach, also useful information on the interposed medium can be obtained.

In the following, an introduction on BSS and on the most used methods will be given. Subsequently, some biomedical applications in the electroencephalography and in the electromyography will be discussed with examples and simulation results.

Chapter 1

Blind Source Separation

1.1 Introduction

An interference signal can be described as a combination generated from the contributions of several sources. If different observations are available, each of them is a mixture of the sources that are weighted by the communication medium and by the distance from the detection point. The most classical example is the cocktail party problem, where many people (the sources) are talking simultaneously in a room and a listener (the observer) is trying to follow one of the discussions: the propagating medium is in this situation the air and the listener's central nervous system (CNS) makes a source reconstruction when he focuses on a single discussion. As will be described in the following, the mathematical methods that have been developed in the field of signal processing require many observations: thus many microphones are used to record the conversations (Figure 1.1).

Referring to the biomedical field, a typical interference signal is the surface electromyogram (EMG), where the sources are the different motor units, the observations are the electrodes placed on the skin and the propagating medium are the interposed tissues. Another example, that is also treated in the following, is the electroencephalogram (EEG), where different sources in the brain in different spatial locations can contribute to the scalp potential.

Source detection can find application in many other situations, from the audio signal processing, where different sources are recorded in acoustic mixtures, to radio communication, where antennas receive different communication signals.

In all the previously mentioned cases, this is an inverse mathematical problem. To solve the inverse problem, different observations are needed: if their number exceeds the number of sources, the model is over-determined and can be solved with linear techniques, otherwise it is an under-determined problem and recovering the solution is a more difficult task.

The term blind source separation (BSS) refers to the source reconstruction based

only on the available observations, assuming limited or no a priori information about the sources and about the communication medium. In the literature different algorithms and approaches have been proposed, to solve both the over-determined and the under-determined case [22], [19]. They all try to recover the sources up to some indeterminacies: in the following, the mathematical model to tackle the problem will be presented and the most popular methods to perform BSS will be discussed.

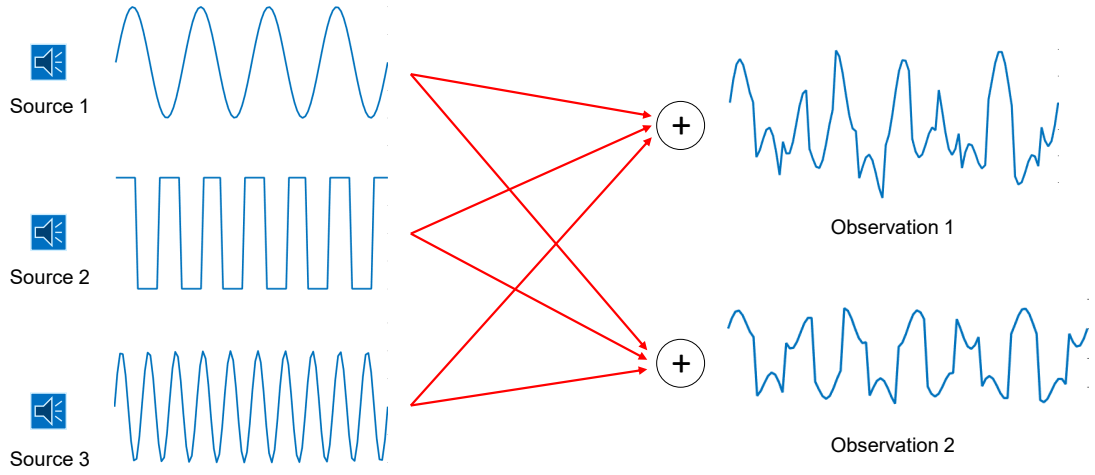

Figure 1.1: *The cocktail party problem, with many speakers talking at the same time and producing different source signals. Two microphones are used to obtain two observations, on which BSS methods can be applied.*

1.2 Methods

To solve the inverse problem of source separation, a mathematical model is needed. The most general is the nonlinear model, where the contributions of the sources add up in a nonlinear way, so they don't follow the superposition principle: as it impossible to solve the inverse problem for such a model, it will not be treated in this work.

Referring to the linear models, for whom the superposition principle holds, they can be classified in two types.

- **Instantaneous linear models**: this model supposes the mixtures $\mathbf{x}(t)$ as linear combinations of the different sources $\mathbf{s}(t)$. The problem is defined as $\mathbf{x}(t) = \mathbf{A}\mathbf{s}(t)$, with mixing weights defined in the matrix $\mathbf{A}$, called mixing

matrix:

$$\mathbf{x}(t) = \begin{bmatrix} x_1(t) \\ \vdots \\ x_m(t) \end{bmatrix} = \begin{bmatrix} a_{11} & \dots & a_{1n} \\ \vdots & \ddots & \vdots \\ a_{m1} & \dots & a_{mn} \end{bmatrix} \begin{bmatrix} s_1(t) \\ \vdots \\ s_n(t) \end{bmatrix} = \mathbf{A}\mathbf{s}(t) \tag{1.1}$$

This model changes the weights in the mixing matrix depending on the distances between sensors and sources. This leads only to an amplitude scaling, depending on relative placement of sources and sensors, and does not consider any filtering effect. Due to these reasons, this model is limited and does not describe properly all the situations.

- **Convolutive linear models**: the model can be written by means of a causal convolution:

$$x(t) = \int A(t-\tau)s(\tau)d\tau \tag{1.2}$$

It has therefore memory of the samples received in the past: the sources are weighted and delayed and contribute to the mixture with multiple samples. The convolutive mixtures take account of the different paths through which the source signals reach the observations across the volume conductor.

In order to consider a more realistic situation, a random noise vector $\mathbf{n}(t)$ is usually added to the previous models: it is typically assumed as a zero-mean, temporally and spatially white process: temporally in the sense that its samples are independent within the same observation, spatially because the noise realizations in different channels are not correlated.

As said before, this is an inverse problem, so mixtures are known. The mixing matrix, the sources and the additive noise are the unknowns. In all the models the mixing matrix has m rows and n columns, where m is the number of sensors and n is the number of sources. The i^{th} column of $\mathbf{A}$ contains the m weights that indicate the contribution of the i^{th} source on each of the channels.

There are two indeterminations in the instantaneous linear model.

1. It is impossible to obtain the amplitude of the sources. Infact, an amplitude scaling of the sources can be corrected with a reciprocal mixing matrix elements scaling:

$$k\mathbf{A}\frac{\mathbf{s}(t)}{k} = \begin{bmatrix} ka_{11} & \dots & ka_{1n} \\ \vdots & \ddots & \vdots \\ ka_{m1} & \dots & ka_{mn} \end{bmatrix} \begin{bmatrix} \frac{s_1(t)}{k} \\ \vdots \\ \frac{s_n(t)}{k} \end{bmatrix} = \mathbf{A}\mathbf{s}(t) \tag{1.3}$$

Exploiting this property, sources are considered with unitary variance by convention: the range of the sources in each mixture is accounted for by the magnitude of the corresponding columns of the mixing matrix $\mathbf{A}$ [2].

2. It is impossible to know the order of the sources. An exchange of place of two sources can be compensated by an exchange of the respective mixing matrix columns.

Given the model, it is then possible to solve the problem. To complete this task, a distance between the estimated sources should be defined and maximized. There are several distance definitions and one of these must be chosen considering prior knowledge about the sources and on the problem formulation.

One of the most used decomposition techniques is the principal component analysis (PCA), which assumes that the sources are not correlated each other, i.e. they are orthogonal. PCA does not belong exactly to the BSS family because it does not reconstruct the original signals, but it is useful for data compression as it mantains the powers of the observations and maximizes the energies of the sources. Another widely used BSS method is the independent component analysis (ICA), which assumes that the sources are statistically independent and minimizes the mutual information between the reconstructed signals. The two approaches are discussed in the following.

1.2.1 Principal Component Analysis

Principal Component Analysis (PCA), also known in the signal processing as discrete Karhunen–Loève transform (KLT), is a statistical procedure based on prior knowledge that the sources are orthogonal between each other: the signal is seen as a linear combination of orthonormal functions, called principal components. Source reconstruction is then performed by minimizing the mean square error (MSE) between the signals $\mathbf{x}_k(t)$ and their reconstructions through the principal components:

$$MSE_i = \frac{1}{T}\sum_{k=1}^{m}\int_0^T \left|x_k(t) - c_{ki}s_i(t)\right|^2 dt \tag{1.4}$$

where $c_{ki}s_i(t)$ is the i^{th} approximation of the k^{th} observation by means of the i^{th} principal component $s_i(t)$. This technique is based on a measure of variance: the data are decorrelated in a second order sense and the new axes result to have a zero dot-product.

For example, given a zero-mean multivariate Gaussian distribution, the two directions of maximum variance, called principal directions, could be identified (Figure 1.2, on the left). The PCA finds them and projects the original observations on these directions in a way that better explains the variance in the data. The distribution after axes rotation is represented in the right on Figure 1.2.

An iterative procedure to reconstruct the principal components is defined from their definition:

1. Compute the first principal component by minimizing Equation (1.4).

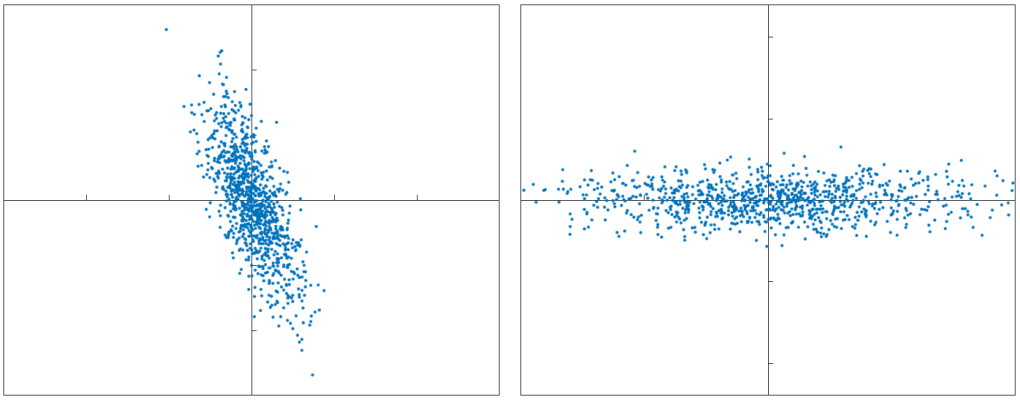

Figure 1.2: *Zero-mean multivariate Gaussian distribution before (left) and after (right) a rotation of the axes performed by the PCA.*

2. Compute the second principal component with the constraint of its orthogonality to the first one.

3. Repeat step 2 until all the m principal components have been reconstructed.

As said before, the principal directions are the directions of maximum variance. Given a set of observations $\mathbf{x}(t)$ and being w_1 a unit norm vector of weights representing the direction of maximum variance, the first principal component is the projection of the data on the first principal direction, i.e. $y = w_1^T x$. The vector w_1 can then be obtained:

$$w_1 = \arg \max_{\|w\|=1} E[(w^T x)^2] \tag{1.5}$$

Maximum variance corresponds to maximum energy. Computed this direction, it is possible to eliminate its information and see the mixtures residual, by subtracting the mixtures projected on the principal component direction from the original mixtures $\mathbf{x}$. Removed the component of the first direction, the second direction of maximum energy can then be obtained by repeating the same procedure, as well as the k^{th} principal direction:

$$w_k = \arg \max_{\|w\|=1} E[w^T (x - \sum_{i=1}^{k-1} w_i w_i^T x)^2] \tag{1.6}$$

It is then possible to do this operation iteratively ending with finding all the directions orthonormal between each other. Now the sources are in order of maximum energy content: if only the first sources are considered, the information is compacted and dimension reduced. As said before, the PCA is not a true source reconstruction technique, but it can be useful when large datasets with many features have to

be processed: by applying the PCA on a training set for a classifier, for example, only the features with higher variance on the new axes can be preserved; this can improve the performances, as features with higher variance are expected to give more information to discriminate between classes. This and many other applications make the PCA a very useful and versatile technique in data processing and machine learning.

Algebraic Method

The covariance matrix $\mathbf{C_{xx}}$, that is symmetric and positive, is defined as:

$$\mathbf{C_{xx}} = \begin{bmatrix} c_{11} & \dots & c_{1M} \\ \vdots & \ddots & \vdots \\ c_{M1} & \dots & c_{MM} \end{bmatrix} \tag{1.7}$$

where each element is the covariance between the i^{th} and the j^{th} observations and the diagonal elements are the variances of each observation.

The mixing matrix $\mathbf{A}$, defined in the previous sections, can be decomposed with eigenvalues and eigenvectors (see APPENDIX):

$$\mathbf{A} = \mathbf{V}\mathbf{L}^{1/2}\mathbf{V}^T \tag{1.8}$$

where $\mathbf{V}$ is a $N \times N$ matrix of eigenvectors and $\mathbf{V}\mathbf{V}^T$ is the identity matrix because $\mathbf{V}$ is a unitary matrix. $\mathbf{L}^{1/2}$ is a square matrix that contains the eigenvalues of $\mathbf{A}$ on the diagonal in descending order. The diagonal form of the covariance matrix then becomes:

$$\mathbf{C_{xx}} = E[\mathbf{x}\mathbf{x}^T] = (\mathbf{A}\mathbf{s} + \mathbf{n})(\mathbf{s}^T\mathbf{A}^T + \mathbf{n}) = \mathbf{A}\mathbf{A}^T + \mathbf{I}_n = \mathbf{V}\mathbf{L}\mathbf{V}^T + \mathbf{I_n} \tag{1.9}$$

where $\mathbf{I_n}$ is the identity matrix multiplied for the covariance of the noise, indicating that it is independent from the channels and has the same power in each observation. The eigenvectors, i.e. the columns of $\mathbf{V}$, correspond to the principal components and the eigenvalues indicate the corresponding power of the sources.

If $M \neq N$, $\mathbf{A}$ is not a square matrix and can be factorized with singular value decomposition (SVD, see APPENDIX):

$$\mathbf{A} = \mathbf{V}\mathbf{\Lambda}^{1/2}\mathbf{U}^T \tag{1.10}$$

where $\mathbf{\Lambda}$ is a $M \times N$ diagonal matrix containing the singular values of $\mathbf{A}$. The

diagonalized covariance matrix then assumes the following form:

$$\begin{aligned}\mathbf{C_{xx}} = E[\mathbf{x}\mathbf{x}^T] = (\mathbf{A}\mathbf{s} + \mathbf{n})(\mathbf{s}^T\mathbf{A}^T + \mathbf{n}) = \mathbf{A}\mathbf{A}^T + \mathbf{I}_n = \\ = \mathbf{V}\mathbf{\Lambda}^{1/2}\mathbf{U}^T\mathbf{U}\mathbf{\Lambda}^{1/2}\mathbf{V}^T + \mathbf{I_n} = \mathbf{V}\mathbf{\Lambda}\mathbf{V}^T + \mathbf{I_n}\end{aligned} \tag{1.11}$$

By considering the eigenvalues or the singular values in descending order, the principal components can then be recovered. It has to be noticed that, for completely recovering $\mathbf{A}$, the matrix $\mathbf{U}$, known as rotation matrix, is needed (the problem will be discussed in more detail in the following).

1.2.2 Independent Component Analysis

Independent component analysis (ICA) is based on the identification of the sources that maintain most of the information. Note that this means that exist directions along which to project the mixtures in order to recover sources that are statistically independent. Given the model $\mathbf{x} = \mathbf{A}\mathbf{s}$, where $\mathbf{x}$ are the available observations, $\mathbf{s}$ and $\mathbf{A}$ are respectively the sources and the mixing matrix, both unknown, the goal is to obtain a demixing matrix such that:

$$\hat{\mathbf{s}} = \mathbf{W}\mathbf{x} \tag{1.12}$$

where $\mathbf{W} = \mathbf{A}^{-1}$ is the inverse of the mixing matrix. If the number of channels m differs the number of sources n, the matrix $\mathbf{A}$ is not invertible and $\mathbf{W}$ is assumed to be its pseudoinverse $\mathbf{A}^{\#}$ (see APPENDIX).

As said before, in the BSS model only the observations $\mathbf{x}(t)$ are available: the basic idea is then to apply some operations to the original data and measure the independence between the obtained signals in order to reconstruct an approximation of the sources $\hat{\mathbf{s}}$.

According to the central limit theorem, the distribution of a sum of independent random variables tends toward a Gaussian distribution: thus, to separate independent sources, gaussianity should be minimized. Different methods have been proposed to obtain a measure of gaussianity.

- **Kurtosis**, which is the fourth statistical moment standardized by the square variance:

$$K(x) = E\left[\left(\frac{x-\mu}{\sigma}\right)^4\right] = \frac{\mu_4}{\sigma^4} \tag{1.13}$$

  where μ_4 is the fourth central moment and σ is the standard deviation. Heavy-tailed distributions, called supergaussian, will have higher kurtosis, while flatter distributions, called subgaussian, will have negative kurtosis (see Figure 1.3).

Equation (1.13) can be rewritten as:

$$K(x) = E[x^4] - 3(E[x^2])^2 \tag{1.14}$$

For a Gaussian distribution, the fourth moment equals to $3(E[x^2])^2$ and Equation (1.14) goes to 0. It is clear that the higher the value of kurtosis, the more the considered variable is distant from a Gaussian distribution.

Kurtosis is a good indicator to discriminate non-gaussian distributions but it is very sensitive to outliars and it is not well suited in noisy measurements.

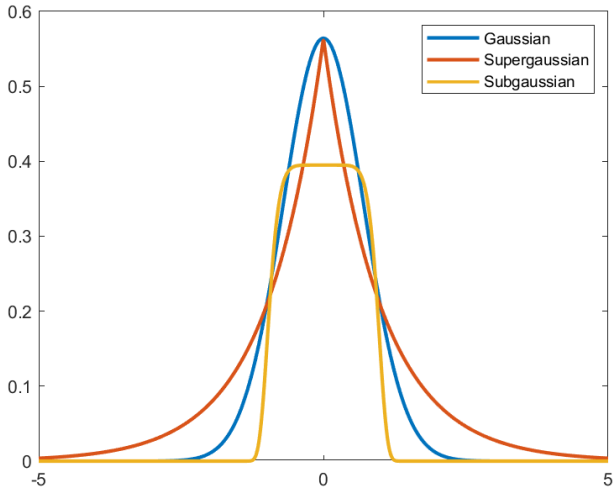

Figure 1.3: *Gaussian, subgaussian and supergaussian distributions.*

- **Negentropy**, that is the difference between the entropy of a Gaussian distribution and that of the considered variable, with the two distributions sharing the same covariance matrix:

$$N(v) = H(G) - H(v) \tag{1.15}$$

where $H(v) = -\int p(v) \ln p(v) dv$ is the entropy of a continuous random variable v, being $p(v)$ its probability density, i.e. the probability at each sample that the random variable could assume that value.

Negentropy vanishes for a Gaussian distribution and has positive values for all the other distributions, as the normal distribution is the one with the highest entropy.

This measuring system is more accurate because it considers all the statistical moments, while kurtosis uses only the fourth one. This difference, however, leads to a greater computational burden for negentropy based algorithms compared to those based on kurtosis.

- **Mutual information**: this measure is based on entropy, which is an information measure. For a set of random variables v_i, $i = 1, \ldots, m$, mutual information is defined as the difference between the entropy of a single variable and the total entropy $H(v)$:

$$I([v_1, \ldots, v_m]) = \sum_{i=1}^{m} H(v_i) - H(v) \tag{1.16}$$

  where $I(v)$ is always positive and equals 0 only when the m variables are independent: it is straightforward that in order to separate the sources, mutual information has to be minimized. Suppose having 2 independent variables v_1 and v_2. The entropy is defined:

$$\begin{aligned} H(v_1, v_2) &= -\int p(v_1, v_2) \ln p(v_1, v_2) dv_1 dv_2 = \\ &= -\int p(v_1)p(v_2) \ln \left(p(v_1)p(v_2)\right) dv_1 dv_2 = \\ &= -\int p(v_1)p(v_2) \ln p(v_1) dv_1 dv_2 - \int p(v_1)p(v_2) \ln p(v_2) dv_1 dv_2 = \\ &= -\int p(v_1) \ln p(v_1) dv_1 - \int p(v_2) \ln p(v_2) dv_2 = H(v_1) + H(v_2) \end{aligned} \tag{1.17}$$

  Total entropy is the sum of two integrals. If v_1 and v_2 are independent, the integrals are their entropies, meaning that there is any cross term: as expected, the mutual information defined in (1.16) would be equal to 0. This measure tells how much information is mutual, which in this case means redundant, as result of the difference between entropies sum and total information.

- **Maximum likelihood estimation**, that it is equivalent to minimize the mutual information. In this sense, latent variables are used to describe the probability distribution of the observations.

  Being $\mathbf{W}$ the unmixing matrix, the log-likelihood is the logarithm of the probability distribution of $\mathbf{x}$, given $\mathbf{W}$. It has the following form:

$$L = \sum_{t=1}^{T} \sum_{i=1}^{n} \log \left\{ p_i[(w_i^T \mathbf{x}(t)] \right\} + T \log |\det \mathbf{W}| \tag{1.18}$$

  where T is the duration of the timeseries, w_i is the i^{th} row of matrix $\mathbf{W}$ and p_i is the probability density of the i^{th} source signal.

Due to the properties defined above, the greater limitation of ICA is clear: Gaussian sources cannot be separated, even if they are independent. The separation with

ICA can be performed only if at most one source in the mixture has a Gaussian distribution. In fact, if all the sources have a Gaussian distribution, any linear combination of them still have a Gaussian distribution, so it is impossible to separate them by trying to make them non Gaussian. In this situation PCA can be used, imposing the sources to be uncorrelated, which is enough for Gaussian variables to be also independent.

ICA can find many applications, for example to remove artifacts from EEG data. A simple simulated example is illustrated in the following (Figure 1.4). Three mixtures, represented in the left of the panel, are generated by applying a mixing matrix to two uniformly distributed sources that simulate EEG recordings and to a low-frequency source that represents an artifact (for example, it can be an ocular artifact generated on electrodes placed in the frontal part of the scalp). The estimated sources, obtained by applying ICA, are superimposed to the simulated ones in the center of the panel. Since the ICA approach contains indeterminacies on the order and on the sign of the sources, the estimated sources were paired with the simulated ones relying on their correlation. On the right the estimated mixtures without the artifact are showed: they were obtained by applying to the sources the estimated mixing matrix with the column corresponding to the source with lowest frequency, that is the artifact, set to zero.

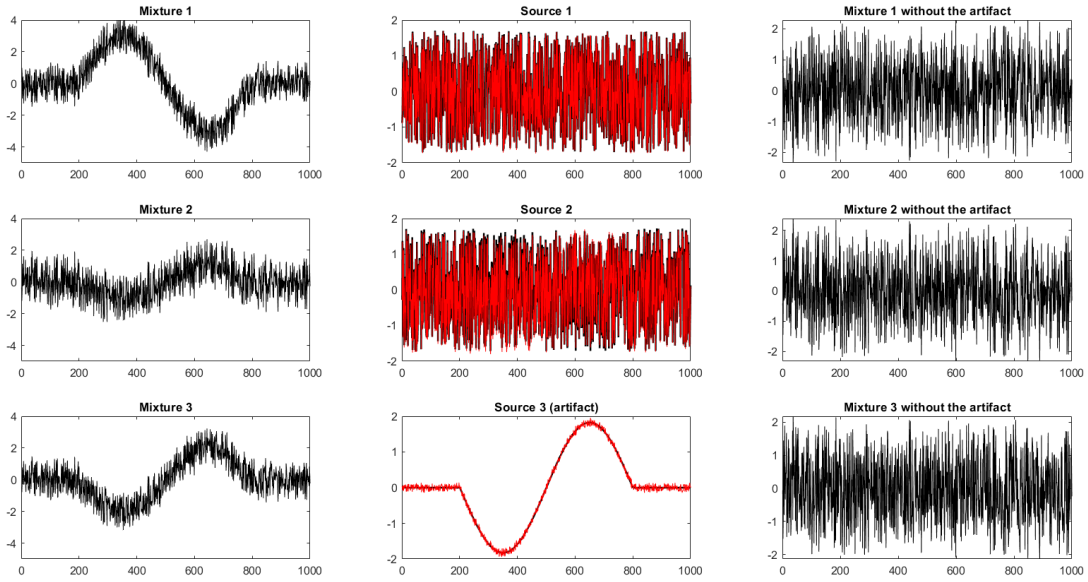

Figure 1.4: *Application of ICA to remove a simulated ocular artifact: on the left the three corrupted mixtures, in the center the estimated sources (in red) superimposed to the simulated ones and on the right the three mixtures after the removal of the artifact.*

In this simple situation, the same solution could have been obtained with a high-pass filter, by removing the low-frequency components. In more complex cases and in the application on real EEG data, however, a filtering approach would bring to a loss of information, as the signal could contain also low-frequency components that are of interest. Moreover, some artifacts are superimposed also in the typical frequency band of the EEG (from 0.01 to around 100 Hz) and this make impossible the use of classical filtering methods without a loss of information [23].

Chapter 2

Inverse Problem in Electroencephalography

2.1 Neurophysiologic introduction of the EEG

The electroencephalogram (EEG) is a monitoring method used to detect electrical activity from the brain. It is typically performed non-invasively with electrodes placed on the scalp, but invasive methods in which electrodes are placed on the cortex, like electrocorticography, are also used.

The EEG is a measure of the difference in voltage between two cerebral locations, plotted over time: it has therefore a good temporal resolution on the electrical changes inside of the brain. In reverse, it has not a high spatial resolution, as it records the contribution of thousands of neurons located in different regions of the brain. The main contribution to the scalp EEG comes from the pyramidal neurons, that are large and have vertically oriented axons.

Neurons generate two types of electrical activity.

- **Action potentials (AP)**, that are brief spikes with a duration of about 1 ms travelling along the neuron axon with great speed ($1 - 100$ m/s). They are involved in neurotransmitters release at the synaptic cleft, which activates the following neuron, called postsynaptic neuron.

- **Post synaptic potentials (PSP)**, that occur when neurotransmitters bind to the receptors in the postsynaptic neuron. PSPs summate both spatially and temporally at the axon hillock and can increase or decrease the probability that the postsynaptic neuron will produce an action potential: in the first case they are named excitatory postsynaptic potentials (EPSP), in the second they are inhibitory postsynaptic potentials (IPSP).

The main contribution to the scalp EEG is given by PSP, as they have longer

duration and can summate. In fact, the dendrites of the postsynaptic neurons are parallely oriented between each other and they are generally perpendicular to the cortical surface on which electrodes are located.

APs can be recorded only if individual neurons fire at exactly the same time, bringing to their summation. Since it's rare for two neurons to fire at the same time and since axons have generally a random orientation, APs usually cancel each other with no contribution to the EEG.

As said before, the EEG has high temporal resolution, but it is poor in spatial resolution: this suggests the benefit of the blind source separation approach, which can bring the information of the main involved areas of the brain when electrical activity is detected, with the excellent resolution of the time activation already provided by the EEG.

2.2 EEG Inverse Problem

Given the measurements at various locations on the scalp, the objective is to find the current sources in the brain that best fit the data. As a limited amount of data is available to reconstruct a model with many unknowns, this is an ill-posed problem: this means that it has not a unique solution and different models can fit equally well the electrode observations. In addition to this, the number of sources is generally much greater then the number of channels, thus the inverse problem is an underdetermined problem. On the contrary, recovering the electrode potentials on the scalp from a given model has a unique solution and it is referred as modelization problem or forward problem.

Different approaches have been proposed in the literature to recover the solution of the inverse problem (a more detailed explanation of the proposed methods can be found in [12]), but they can be summarized in three main types.

- **Equivalent current dipoles (ECD)**, where the electrical activity is thought as the product of a discrete number of dipoles. The basic idea is to compute the potential distribution on the scalp for different positions in the brain of hypothetical current dipoles and try to fit it to the original data.
- **Distributed sources**, where all source locations are considered simultaneously. This model is more accurate, as the activity is in general spread throughout the brain and not only in discrete points.
- **Beamformers**, that consider time-varying dipoles and perform a spatial filtering trying to mantain only the signals that come from the sources of interest.

The forward problem, i.e. the potential distribution on the scalp due to some known source positions, is therefore computed, once or many times depending on the used approach, and then it is used to derive the true source locations by fitting

the potential to the electrode measurements at specified positions. In order to solve such a problem, a proper head model, that takes account of the different tissues in which the potential propagates, is needed, as well as the electrode positions on the scalp. Note that also small errors in the head or in the source modelling and the presence of noise can bring to wrong results in the inverse problem. When are available, anatomical headmodels based on a patient magnetic resonance image (MRI) can highly improve the goodness of the solution.

Another important step in approaching to the inverse problem are the constraints on the sources, that simplify the search for a solution and make it solvable. An interesting example is the use of functional magnetic resonance imaging (fMRI) in order to detect the activation areas in the brain during a certain task [7]. The fMRI has high spatial resolution but poor temporal resolution, thus its combination with source reconstruction allows to obtain high resolution spatio-temporal maps of the neural activation.

The main steps to perform source reconstruction from EEG data are summarized in Figure 2.1, while an example of headmodel and electrode positions are showed in Figure 2.2. The headmodel was created with a three-shell mesh containing the brain (in red), the skull and the scalp, while the electrodes (corresponding to a standard 10-20 placement) were plotted on the scalp layer.

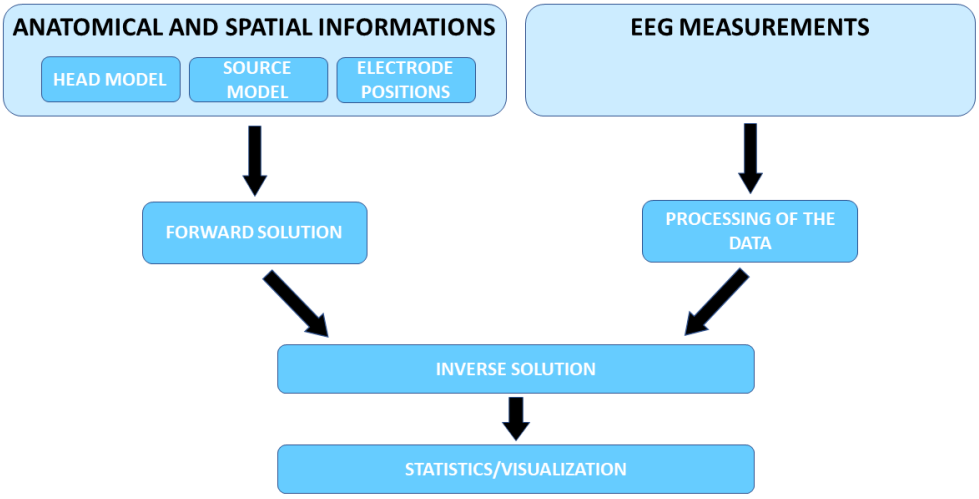

Figure 2.1: *Typical procedure for source reconstruction from EEG data.*

Source detection in the EEG can find many applications, from artifact removal (e.g. ocular artifacts that result to be located in the anterior part of the scalp and are then easily recognized) to surgical intervention in the focus of seizure activity.

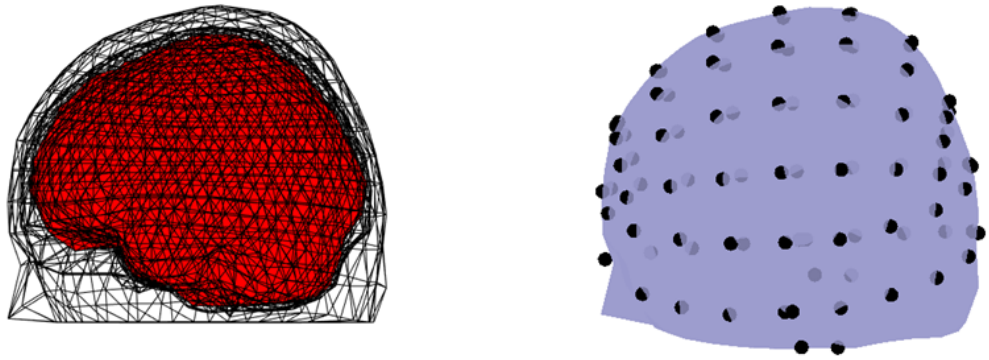

Figure 2.2: *Mesh of a three shell head model (left) and electrodes plotted on the cortical surface (right).*

The knowledge of the position of a given source can also provide a better understanding of the complex dynamics of the brain areas involved in different cognitive tasks.

2.2.1 Mathematical Formulation

Suppose that k electrode measurements are available in the matrix $\mathbf{M}$:

$$\mathbf{M} = \mathbf{GD} + \mathbf{n} \tag{2.1}$$

where each row of $\mathbf{G}$ describes the current flow through the j^{th} electrode caused by each one of the different dipoles and is called lead-field, $\mathbf{D}$ contains the dipole moments at different time instants and $\mathbf{n}$ is additive noise. The dipole moment mentioned before is composed by two angles that define the orientation in the space and by a scalar that defines its strength. By neglecting the noise, the problem can then be written in the following extended matrix form:

$$\mathbf{M}(r,t) = \begin{bmatrix} m(r_1,t) \\ \vdots \\ m(r_k,t) \end{bmatrix} = \begin{bmatrix} g(r_1, r_{dip_1}) & \dots & g(r_1, r_{dip_p}) \\ \vdots & \ddots & \vdots \\ g(r_k, r_{dip_1}) & \dots & g(r_k, r_{dip_p}) \end{bmatrix} \begin{bmatrix} d_1 e_1 \\ \vdots \\ d_p e_p \end{bmatrix} \tag{2.2}$$

where $d_i = (d_{ix}, d_{iy}, d_{iz})$ is a vector of the magnitude components of the considered dipole and $e_i = \frac{d_i}{|d_i|}$ defines its orientation. Note the dependence on time and on the electrode locations given by r_j and the six unknowns that are the three spatial coordinates of r_{dip_i}, the two orientation angles θ and ψ that define the dipole moment and the scalar $d = |d_i|$ that defines its strength. Under these assumptions, recovering the solution is a very complex task: as said before, different approximations

and constraints were then proposed in order to simplify the problem. For example, since the apical dendrites that generates the field are normally oriented to the scalp surface, dipole orientation can be constrained to such direction: thus, once discrete positions in the brain are assumed, only the dipole strengths d_i will vary in the formulation of Equation (2.2). Since the EEG inverse problem is ill-posed, a regularization is needed: this means to use some a priori constraints about the sources in order to reduce the vagueness and recover the solution. This balance the fidelity to the data with spatial and temporal smoothness, depending on the priors. Different regularization approaches were proposed, for example maximum entropy metrics, L_1 norm and L_2 norm: the correct choice depends on the particular conditions and on the characteristics of the sources (for example, the use of L_1 norm favors the detection of sparser solutions).

Now that the model has been defined and the variables that play a role in the EEG inverse problem have been shown, two of the main methods to recover the solution are discussed in more detail.

2.2.2 Equivalent Current Dipoles

The equivalent current dipole (ECD) approach is based on the assumption that if the activity is early and not spread in the brain, an equivalent current dipole is a reasonable approximation. Therefore the ECD formulation, also known as dipole fitting, assumes that an equivalent current dipole is able to describe the measured scalp topography [21]. Given the electrode measurements and the head model, as described in the previous, the inverse problem can then be solved by discretizing the brain with a point-grid, where at each point the forward solution is computed for a dipole placed at that location.

It is clear that a higher resolution of the grid increases the performance of the source detection, but also increases the processing time. This also suggests why only a single dipole could be fitted to a considered scalp topography: by using for example a grid with 5000 points, if for each computed forward solution the presence of another dipole should be taken into account, there would be $5000 \cdot 5000 = 25 \cdot 10^6$ possible combinations for which the solution has to be computed! If more than one dipole is needed, the only way is then to place a constraint on the second dipole by imposing its symmetry to the first one.

Dipole fitting finds the current dipole that best fit the data in a least square sense. This means that the obtained solution only partially explain the measured potential, since it always has a residual variance.

Due to the limitations discussed above, the most common approach is to obtain a large number of event-related potentials (for example from a task related activity) and then apply the dipole fitting to the average of the trials. Another useful method in this situation is the ICA: by decomposing the original EEG data into independent components, each of them can then be fitted with an equivalent current dipole

[26]. This is reasonable because the timecourse of an independent component could generally be thought as the product of a small number of sources in the brain with a well localized spatial activity [9].

Figure 2.3 shows a simulated example on a standard MRI headmodel. Four signals were generated: three of them were random noise, while the fourth was obtained by computing the forward solution for a dipole placed in the left prefrontal cortex. With the application of ICA, the four components were separated and the one containing the signal of interest could then by fitted with an ECD.

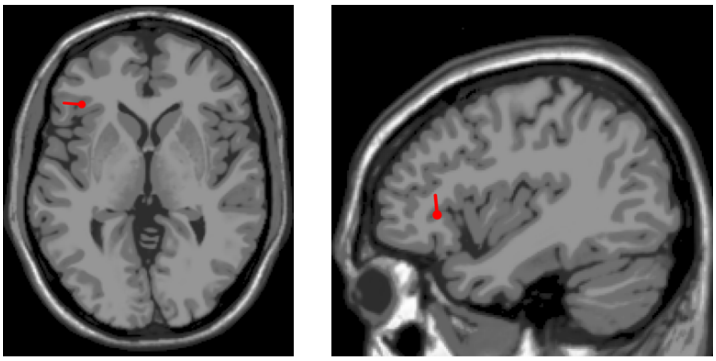

Figure 2.3: *Reconstruction of an equivalent current dipole in the left prefrontal cortex.*

2.2.3 Distributed Source Models

If the measured scalp activity cannot be traced with a single dipole, a more robust approach is needed in order to fit a distributed activation pattern to the data. Most of the methods used to fit distributed sources derive from the Bayesian framework, that consists in finding an estimator that maximizes the posterior probability of the sources $\mathbf{s}$, given the measurements $\mathbf{M}$:

$$\hat{\mathbf{s}} = \max_{\mathbf{s}}[p(\mathbf{s}|\mathbf{M})] \tag{2.3}$$

where $p(\mathbf{s}|\mathbf{M})$ is the conditional probability of the sources for the set of observations.

By exploiting Bayes' law, this conditional probability can be rewritten as:

$$p(\mathbf{s}|\mathbf{M}) = \frac{p(\mathbf{s})p(\mathbf{M}|\mathbf{s})}{p(\mathbf{M})} = \frac{\exp\left[-F_\alpha(\mathbf{s})\right]/z}{p(\mathbf{M})} \tag{2.4}$$

where z is the partition function (i.e., a normalization constant), $F_\alpha(\mathbf{s}) = U_1(\mathbf{s}) + \alpha L(\mathbf{s})$ where $U_1(\mathbf{s})$ and $L(\mathbf{s})$ are energetic functionals associated to $p(\mathbf{M}|\mathbf{s})$ and $p(\mathbf{s})$ respectively and α is a regularization parameter. Specifically, $U_1(\mathbf{s})$ can be

written as $\|\mathbf{Ks} - \mathbf{M}\|^2$, where K is a compact linear operator representing the forward solution and $L(\mathbf{s})$ is chosen to introduce spatial (anatomical) and temporal constraints. The sources are then estimated by minimizing $F_\alpha(\mathbf{s}) = U_1(\mathbf{s}) + \alpha L(\mathbf{s})$:

$$\hat{\mathbf{s}} = \min_{\mathbf{s}}(\|\mathbf{Ks} - \mathbf{M}\|^2 + \alpha L(\mathbf{s})) \tag{2.5}$$

By using the notation with which the inverse problem was described, the following equation is obtained:

$$U(\mathbf{D}) = \|\mathbf{M} - \mathbf{GD}\|^2 + \alpha L(\mathbf{D}) \tag{2.6}$$

where the first term reflects fidelity to the data and the second one introduces spatial and anatomical priors. Different choices of the regularization function $L(\mathbf{D})$ were proposed, bringing to different approaches.

Minimum norm estimates (MNE) perform a search for the solution with minimum power. This corresponds to Tikhonov regularization and it is well suited for sources that are distributed in some areas of the cortical surface. This approach considers the following regularized problem:

$$U(\mathbf{D}) = \|\mathbf{M} - \mathbf{GD}\|^2 + \alpha\|\mathbf{D}\|^2 \tag{2.7}$$

which leads to the following solution:

$$\mathbf{D_{MNE}} = (\mathbf{G^T G} + \alpha\mathbf{I_N})^{-1}\mathbf{G^T M} \tag{2.8}$$

Another possibility is choosing:

$$L(\mathbf{D}) = \|\mathbf{AD}\|^2 \tag{2.9}$$

where $\mathbf{A}$ is a linear operator (e.g., for sampled data, it is a matrix, which could discretize different operators; for example, if it samples the derivative operator, the solution is constrained to be smooth; if only the energy of the solution should be penalized, $\mathbf{A} = \mathbf{I}$). In this case, the solution is:

$$\mathbf{D_{MNE}} = (\mathbf{G^T G} + \alpha\mathbf{A^T A})^{-1}\mathbf{G^T M} \tag{2.10}$$

An example of source reconstruction with MNE is represented in Figure 2.4, where a small number of dipoles in the right prefrontal cortex were simulated by computing the forward solution for nearby locations. The signals were then summed up on the electrodes in order to produce a distributed activity. Note that the obtained map contains the power of the activity in each point of the grid. The

solution perfectly fits the measured potential and since the non-uniqueness of the inverse problem, it is that with lower energy (minimum norm).

Another choice of the linear operator $\mathbf{A}$ brings to the low resolution electrical tomography (LORETA), which combines the lead-field normalization with the Laplacian operator: by normalizing the columns of $\mathbf{G}$ it gives all the sources the same importance, then deeper sources have the same possibility to be recostructed as the more superficial ones. Note that the Laplacian operator gives smoothness in the inverse solution: this type of regularization can then bring to problems due to spatial blurring, with lower spatial resolution.

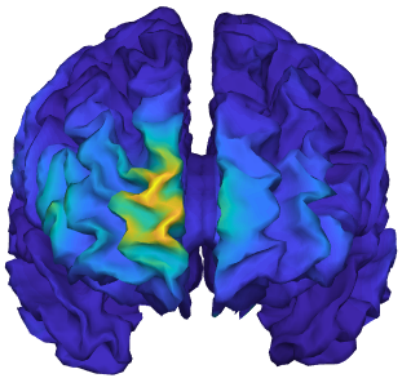

Figure 2.4: *MNE source reconstruction of a simulated activity in the prefrontal cortex.*

Chapter 3

EMG Decomposition

3.1 The Surface Electromyogram

Muscle contraction is performed in response to stimuli from the central nervous system (CNS). The neural drive passes from the spinal circuitries to the peripheral nervous system (PNS), where thousands of motor neurons interact in the generation of the motor commands. Each motor neuron (MN) projects the electrical activity on several muscle fibers, thus this activity is amplified at the muscle level. The electrical signals propagate along nerve fibers and reach the neuromuscolar junction (NMJ), where they excite the innervated muscle fibers: the depolarization of each of these fibers is called single fiber action potential (SFAP). The summation of all the SFAPs belonging to the same MN gives rise to the motor unit action potential (MUAP).

As said before, a single neural command from the CNS generates a widespread electrical activity at the muscle level: it is therefore possible to study the neural activation directly and non-invasively from the surface of the skin through high density measurements, as the surface electromyogram (sEMG). Surface EMG is a high resolution acquisition techinique that allows to arrange multiple electrodes in two-dimensional arrays, providing high information on the spatial variability of the electrical activity. A large number of observations (mixtures) is then available and the signals can be investigated at different levels.

- **Muscle synergies:** the CNS coordinates the motor activation in a task related manner, as the number of muscles largely exceeds the number of joints. Hence, a group of muscles can be recruited to perform the same movement. Therefore, by detecting the primitive signals entailed in the activation of multiple muscles, the complex activation pattern that generates a movement could be better understood.

- **Single muscles:** the muscle of interest can be isolated from the activity of

the other muscles. Thus cross-talk, i.e. the interference of the nearby muscles, can be avoided by considering each muscle as an independent source and by applying a BSS method, like ICA or PCA.

- **Motor unit (MU):** MUs are the smallest functional units in a movement task and are composed by a motor neuron and the muscle fibers it innervates with its axonal terminals. The MUAPs that they generate superimpose in space and in time: thus they can be viewed as the sources and their timecourses can be recovered from the interference EMG of a muscle.

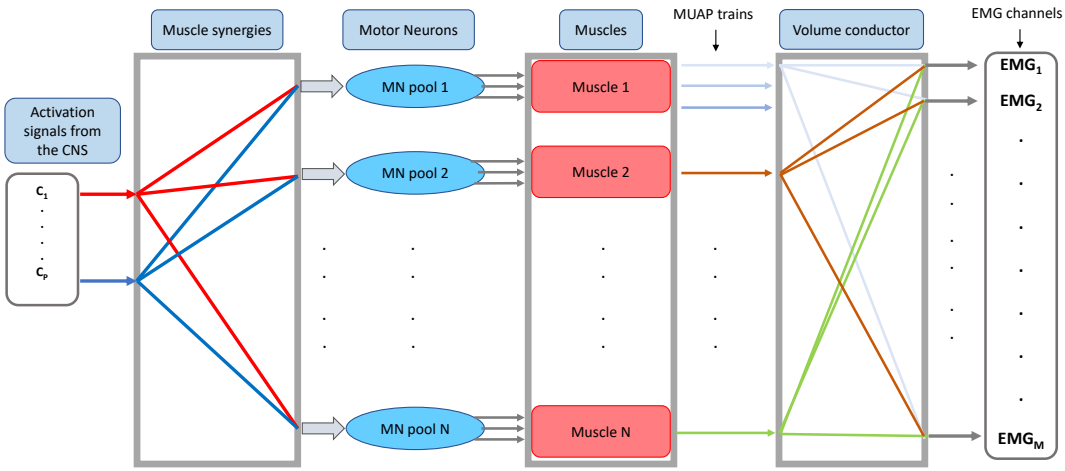

Figure 3.1: *Multi scale model of movement generation: from the left, the signals arising from the CNS are taken as input from different motor neurons. Each MN innervates a large number of fibers of a muscle with multiple spike trains, giving rise to different motor units. The contribution of different MUAP trains is picked up by the electrodes weighted by the conduction medium, as can be seen in the right of the figure.*

Depending on the prior assumptions and on the sources of interest, the surface EMG signals can be viewed both as linear instantaneous or convolutive mixtures. For example, for the separation of individual MUAPs, a convolutive mixing model is assumed, as the instantaneous model is not well suited for taking account of the orientation of the muscle fibers and of the low-pass filtering effect of the volume conductor that modifies the shapes of the MUAPs. Conversely, if the interest is focused on the separation of single muscles and on the cross-talk, the instantaneous mixing model is a good approximation and has been successfuly used to describe the problem [11].

In the following sections, three applications of the blind source separation in the decomposition of EMG signals will be showed: the first one is related to the

separation of the contributes of nearby muscles, thus reducing cross-talk, while the last two are methods to decompose the surface EMG at the motor unit level.

3.2 Separation of Single Muscles

When the EMG signal is acquired with electrodes placed on a muscle, also the contribution of nearby muscles is detected (Figure 3.2). By using a proper spatial filter, as single differential (SD), double differential (DD) or the Laplacian operator, selectivity can be increased, but it leads to a reduced spatial detection with a smaller contribution also of the motor units of the considered muscle.

The cross-talk, i.e. the contribution of a muscle that is not the one of interest, is still an open problem that highly affects the EMG acquisition: as the source signals are in general overlapped both in time and in frequency, linear filtering techniques are not suitable to separate them. The BSS approach, instead, can help to overcome the problem: the two muscles can be treated as independent sources and their contributions can be separated.

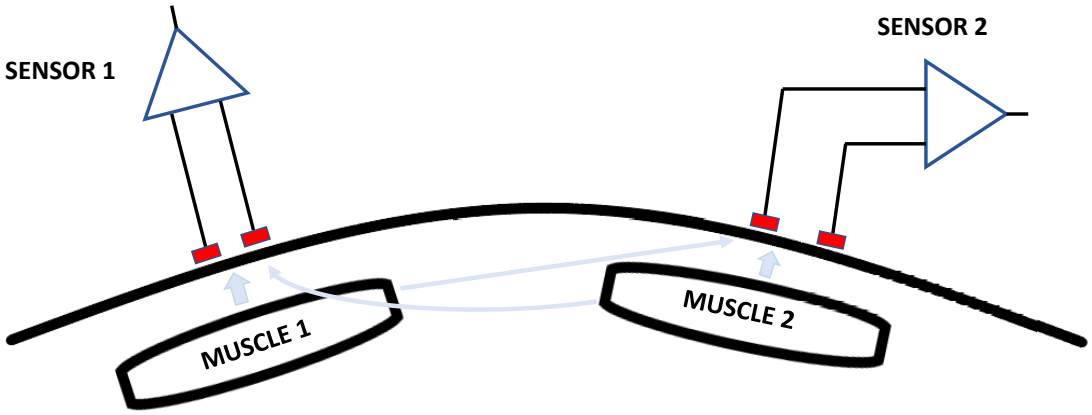

Figure 3.2: *EMG acquisition on two muscles. Each sensor detects the contribution both of the muscle on which it is placed on and of the nearby muscle.*

One of the first approaches to the blind separation for cross-talk reduction was proposed in [2]. The method, called second order blind identification (SOBI), extends the PCA by applying a whitening transformation and then by recovering the rotation matrix $\mathbf{U}$. In order to obtain a better estimate of $\mathbf{U}$, a set of covariance matrices (for different delays τ) is jointly diagonalized instead of a single covariance matrix. Another approach, derived from the SOBI, is to perform the joint diagonalization to a set of spatial time-frequency distributions (STFD), that are defined as the Fourier transform in the delay τ of the covariance matrices [3]. The latter,

by exploiting the information given by the non stationarity of the sources, can overcome some limits of the first approach in separating signals with the same spectral shape, since the spectral contents can have different locations in the time-frequency plane.

Concerning the SOBI method, it is based on the following steps:

- **Whitening**: as in the application of the PCA, a whitening matrix $\mathbf{W}$ is constructed such that:

$$E[\mathbf{W}\mathbf{y}(t)\mathbf{y}(t)^T\mathbf{W}^\mathbf{T}] = \mathbf{W}\mathbf{C}_y(0)\mathbf{W}^\mathbf{T} = \mathbf{W}\mathbf{A}\mathbf{A}^\mathbf{T}\mathbf{W}^\mathbf{T} = \mathbf{I} \tag{3.1}$$

  where $\mathbf{y}(t)$ is the signal part of the observations, i.e. $\mathbf{x}(t)$ without the noise contribute and $\mathbf{C}_y(0) = \mathbf{A}\mathbf{A}^\mathbf{T}$ because the sources are assumed to be uncorrelated (i.e. $\mathbf{C}_s(0) = \mathbf{I}$). The matrix $\mathbf{W}$ is a whitening matrix (see APPENDIX), then $\mathbf{W}\mathbf{A} = \mathbf{U}$ is a $N \times N$ unitary matrix (i.e. $\mathbf{U}^\mathbf{T}\mathbf{U} = \mathbf{U}\mathbf{U}^\mathbf{T} = \mathbf{I}$) such that:

$$\mathbf{A} = \mathbf{W}^\#\mathbf{U} \tag{3.2}$$

  where $\mathbf{W}^\#$ is the Moore-Penrose pseudoinverse of $\mathbf{W}$ (see APPENDIX).

  Then, if a noise estimate is available and with the previously mentioned assumption that the sources are uncorrelated, the matrix $\mathbf{W}$ can be computed directly by the covariance matrix of the observations at zero lag:

$$\mathbf{A}\mathbf{A}^\mathbf{T} = \mathbf{C}_\mathbf{x}(0) - \sigma_n^2\mathbf{I} \tag{3.3}$$

  where σ_n^2 can be estimated from the average of the $M-N$ smallest eigenvalues of the covariance matrix. Note that this procedure extends the PCA by scaling the whitened components by a factor $(\lambda_i - \sigma_n^2)^{1/2}$, where λ_i are the eigenvalues of the covariance matrix $\mathbf{C}_\mathbf{x}$.

- **Determination of the rotation matrix.** It is clear that for completely recovering the mixing matrix $\mathbf{A}$, the rotation matrix $\mathbf{U}$ is needed. Considering the whitened covariance matrices for different delays $\tau \neq 0$:

$$\hat{\mathbf{C}}(\tau) = \mathbf{W}\mathbf{C}_\mathbf{x}(\tau)\mathbf{W}^\mathbf{T} = \mathbf{W}\mathbf{A}\mathbf{C}_\mathbf{s}(\tau)\mathbf{A}^\mathbf{T}\mathbf{W}^\mathbf{T} \tag{3.4}$$

  and then by using the (3.2), the previous relation becomes:

$$\hat{\mathbf{C}}(\tau) = \mathbf{U}\mathbf{C}_\mathbf{s}(\tau)\mathbf{U}^\mathbf{T} \tag{3.5}$$

It is then clear that for recovering the unitary matrix $\mathbf{U}$, the whitened covariance $\hat{\mathbf{C}}$ has to be diagonalized for some delay τ. This can be done as:

$$\mathbf{C_s}(\tau) = \mathbf{U^T}\hat{\mathbf{C}}(\tau)\mathbf{U} \tag{3.6}$$

In principle, it could be diagonalized for any delay τ, even if more stable alternatives were obtained by sampling more time lags and choosing the matrix providing their best joint diagonalization under some optimality condition. A proper choice of the delay can be satisfied for example by minimizing the sum of the non-diagonal elements of the source covariance matrices obtained by performing the diagonalization in (3.5). The choice of different delays is justified by the fact that it improves the robustness of the algorithm and avoids that an unlucky selection of a single delay could bring to wrong results.

In the example of Figure 3.3, two distinct muscles were simulated with respectively 20% and 60% maximal voluntary contraction (MVC). Three mixtures were available, taken from two electrodes placed on each one of the two muscles (with the cross-talk contribution of the other source) and from an electrode placed between them: the SOBI method was applied to the mixtures in order to recover the original signals of the two muscles. Note the partially overlapped spectra, that would make very complicated the separation with classical filtering techniques.

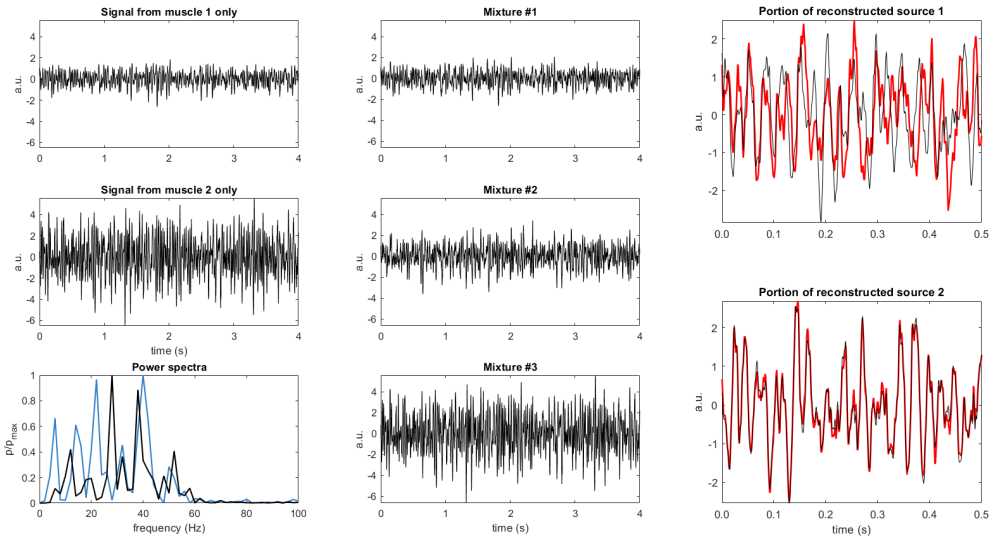

Figure 3.3: *SOBI method applied to reduce cross-talk between two muscles with partially overlapping spectra. The simulated monopolar signals with their power spectral densities are showed in the left portion of the panel, the three mixtures are in the middle and the result of the reconstruction (in red) superimposed to the muscles original signals is showed on the right.*

3.3 Separation of Motor Unit Action Potentials

MU decomposition is the process of recovering individual MU activities from the interference EMG, where they are superimposed both spatially and temporally. The investigation at MU level can provide both physiological and diagnostic understanding on neuromuscular activity, for example in the detection of neuromuscular disorders.

Since the number of motor units largely exceeds the number of available observations, MU decomposition is a challenging task, even for a manual expert editing. Early work also involved template-matching approaches, that focus on the shape of the MUAP waveforms. All previous methods could only detect a limited number of MUs, as it is difficult to resolve the superposition of a large number of waveforms.

Since MUAPs are generated from different motor units, they discharge with a small degree of synchronicity in case of low or moderate levels of force: the hypothesis of independence is then satisfied, so the EMG decomposition at the MUAP level can be successfully carried out with BSS. Independent component analysis, for example, can be used to separate the contibutions from different MUAPs in order to detect they discharge timings [5]. Other methods have been proposed in the literature, as the convolution kernel compensation [13], where the mixing matrix $\mathbf{A}$ is compensated in order to recover the source trains only.

In the next sections, the convolutive model used for the surface EMG data is presented. Subsequently, a brief introduction on the convolution kernel compensation will be given and a new algorithm, based on ICA [5], will be explained with simulation results.

3.3.1 Data Model

The convolutive model is here explained in the case of the surface EMG: the electrode observations can be thought as linear weighted sums of different source signals, where each signal is a firing train belonging to a different MU. As said in the first chapter, the model results in a causal convolution (Equation 1.2), where each MUAP train is described as the convolution of the MUAP with a pulse train (that is in general a series of Dirac deltas indicating the MU firing times).

Assuming M discrete-time observations, each of them being a mixture of N different sources of L samples length, the convolutive mixture can be extended to the following matrix form:

$$\mathbf{x}(t) = \mathbf{A}\mathbf{s}(t) + \mathbf{n}(t) \tag{3.7}$$

where $\mathbf{x}(t) = [x_1(t), x_2(t), \ldots, x_M(t)]^T$ is a vector containing all the mixtures, as taken by each of the M electrodes, $\mathbf{s}(t) = [s_1(t), s_1(t-1), \ldots, s_1(t-L), s_2(t), s_2(t-$

$1), \ldots, s_2(t-L), \ldots, s_N(t), \ldots, s_N(t-L)]^T$ is a vector containing the N sources, each of them with L delayed replicas in order to allow matrix multiplication and $\mathbf{n}(t)$ is zero-mean white Gaussian noise. The mixing matrix $\mathbf{A}$ contains the different MUAP waveforms as picked up by each electrode:

$$\mathbf{A} = \begin{bmatrix} a_{11} & \ldots & a_{1N} \\ \vdots & \ddots & \vdots \\ a_{M1} & \ldots & a_{MN} \end{bmatrix} \tag{3.8}$$

where $a_{ij} = [a_{ij}(1), a_{ij}(2), \ldots, a_{ij}(L)]$ is the waveform of the j^{th} muap, as detected by the i^{th} electrode.

The surface EMG recordings were simulated through the convolutive model explained above. Randomly generated firing trains, composed by 0 or 1, the second standing for MU discharge times, were convoluted with different MUAP waveforms that take account of the scaling between each electrode observation and of the different shapes of the MU spikes. Different contraction levels can be simulated by increasing the number of active MU (spatial recruitment) and the number of spikes in each train (the firing rate, that reflects temporal recruitment). The MUAP discharge patterns, resulting in a $M \times T \times N$ matrix, where M are the available observations, T is the length in time of the signals and N is the number of active MUAPs, were then summed to obtain the mixtures on the electrodes (a matrix with 63 electrodes was assumed, see Figure 3.4).

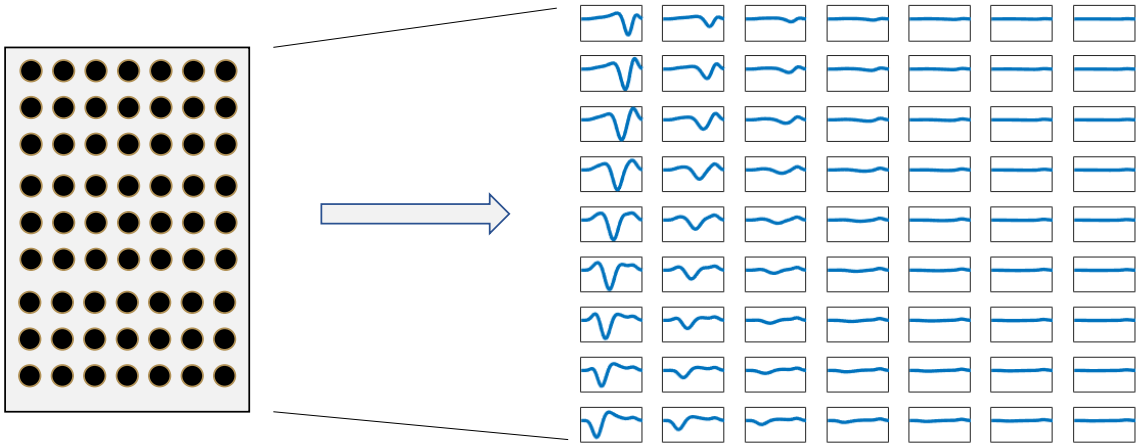

Figure 3.4: *The 9×7 electrode grid with a single MUAP waveform, as detected by each one of the electrodes.*

3.3.2 Convolution Kernel Compensation

As said before and based on the proposed model, the MUAP trains can be considered as uncorrelated pulse sequences. With this assumption, the convolution kernel compensation (CKC) focuses on the pulse trains only and tries to compensate the contribution of the mixing matrix $\mathbf{A}$, with no interest in the reconstruction of the last one. The MUAP waveforms, i.e. the kernels, could be subsequently obtained by spike triggered averaging, after recovering the pulse trains.

The original observations are extended with $K-1$ delayed replicas, such that the extended matrix $\bar{\mathbf{x}}$ contains $M \cdot K$ rows. The mixing matrix of Equation (3.8) then becomes a $KM \times N(L+K-1)$ block matrix, where each block $\mathbf{A_{ij}}$ is called convolution kernel and is defined as:

$$\mathbf{A_{ij}} = \begin{bmatrix} a_{ij}(0) & a_{ij}(1) & \dots & a_{ij}(L-1) & 0 & \dots & 0 \\ 0 & a_{ij}(0) & \dots & a_{ij}(L-2) & a_{ij}(L-1) & \dots & 0 \\ \vdots & \ddots & \ddots & \ddots & \ddots & \ddots & \vdots \\ 0 & \dots & 0 & a_{ij}(0) & \dots & a_{ij}(L-2) & a_{ij}(L-1) \end{bmatrix} \tag{3.9}$$

Each convolution kernel contains the contribution of the j^{th} source and its $K-1$ delayed replicas, since by extending the i^{th} electrode observation, also the sources are extended.

The method is here explained in the overdetermined case, assuming that the number of observations exceeds the number of sources, but it can be extended to the underdetermined case mantaining good performances if the extension factor is large enough to guarantee $N(L+K-1)/KM < 2$.

The convolution kernels are compensated by computing the activity index, that can be seen as a global indicator of the pulse train activity:

$$\begin{aligned} \gamma(t) &= \bar{\mathbf{x}}^T(t)\mathbf{C}_{\bar{x}\bar{x}}^{-1}\bar{\mathbf{x}}(t) \\ &= \bar{\mathbf{s}}^T(t)\mathbf{A}^T(\mathbf{A}^T)^{-1}\mathbf{C}_{\bar{s}\bar{s}}^{-1}\mathbf{A}^{-1}\mathbf{A}\bar{\mathbf{s}}(t) \\ &= \bar{\mathbf{s}}^T(t)\mathbf{C}_{\bar{s}\bar{s}}^{-1}\bar{\mathbf{s}}(t) \end{aligned} \tag{3.10}$$

where $\mathbf{C}_{\bar{x}\bar{x}}^{-1}$ and $\mathbf{C}_{\bar{s}\bar{s}}^{-1}$ are the inverse of the correlation matrices respectively of the extended observations and of the extended sources, the first being calculable from the original data as $\mathbf{C}_{\bar{x}\bar{x}} = E[\bar{\mathbf{x}}(t)\bar{\mathbf{x}}^T(t)]$. Then, being t_0 a time instant when only a single train is active, its timecourse can be reconstructed by using $\bar{\mathbf{x}}^T(t_0)$ as premultiplying vector in Equation (3.10).

Since finding a time instant with no overlapping pulses is not an easy task, a probabilistic approach is used by starting from the median argument of the activity index γ and by computing all the possible products combinations between a number R of reconstructed trains and finding the pulses that exceed a predefined threshold.

The CKC is an iterative procedure, as after a MUAP has been reconstructed, its discharge timings are set to 0 in the activity index and the method is applied again in this way until all the MUAP trains have been reconstructed.

3.3.3 ICA Decomposition

Individual motor unit discharge timings were reconstructed through the application of ICA and k-means clustering, as described in [5]. The following ICA-based algorithms were evaluated.

- **Infomax**, that is based on the maximization of mutual information between the input and the output of a neural network. The method minimizes the mutual information between the sources [1].
- **FastICA**, that minimizes gaussianity through a measure of negentropy [14].
- **RobustICA**, that uses a kurtosis contrast function [25].

The three algorithms are available in EEGLAB [8], an open source toolbox that provides a graphical user interface and built-in functions that can be easily integrated in custom made Matlab scripts.

The k-means clustering was used after the application of ICA because each independent component does not necessarily contain a single MU discharge sequence, as the number of sources could be much higher than the number of electrodes (underdetermined case). In order to obtain a valid value for the number of clusters, the algorithm requires as input the approximate mean number of spikes of the MUAP trains. An example of ICs probably containing more then a single MUAP timecourse is shown in Figure 3.5, where ICs 2 and 4 do not present a single and distinct pattern in the peaks distribution: in these situations the application of a clustering algorithm is crucial in order to correctly detect at least a MUAP train. For each IC, the value of kurtosis is also showed: as expected, ICs 2 and 4 have the smallest values, indicating that they are closer to a Gaussian distribution. This is consistent with what was said in Chapter 1, as the sum of more variables is more Gaussian then a single variable, thus reflecting in a smaller value of kurtosis. Note also the small delay of IC 5 with respect to IC 6, indicating that they contain the same MUAP with a few samples of delay. This is caused by the extension factor, that by increasing the number of observations, also increases the number of sources.

The main steps of the decomposition are here summarized:

1. Extend the EMG signals by adding $K - 1$ delayed replicas to each row, such that the matrix $\mathbf{x}$ is now composed by M blocks of K observations.
2. Whiten the signals using singular value decomposition (SVD). This means applying a premultiplying matrix $\mathbf{T}$ to the data such that the obtained observations $\mathbf{x_w} = \mathbf{Tx}$ have a covariance matrix equal to the identity matrix $\mathbf{I}$. The

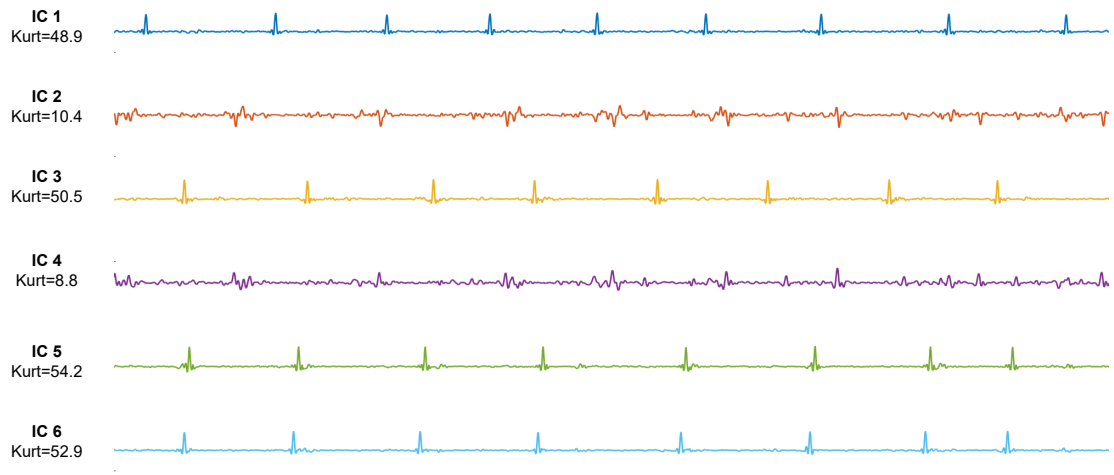

Figure 3.5: *Example of portions of ICs obtained by applying ICA. For each IC the value of kurtosis is indicated. ICs* $1, 3, 5$ *and* 6 *clearly show a single MUAP shape repeated over time, while in ICs* 2 *and* 4 *is more difficult to find a single MUAP train.*

rows of $\mathbf{x}$ are then decorrelated (see APPENDIX).

3. Apply one of the ICA algorithms to the whitened signals.

4. Given the $M \cdot K$ obtained independent components, identify the discharge timings through peak detection and classify them through k-means. This is an iterative operation, where for each iteration the independent components are scanned one by one and their peaks, both positive and negative, are detected and given as input to k-means. The number of obtained clusters is defined as $k = n/spike\_th$ rounded to the smallest interger, where n is the number of detected peaks and $spike\_th$ is the threshold on firing events provided as input to the decomposition algorithm. Only the most homogeneous cluster is mantained and added to the output. Before starting the next iteration searching for another possible firing pattern, the peaks in the detected discharge timings are subtracted from the corresponding IC.

5. Remove the duplicate trains, as the presence of the delayed replicas could bring to the identification of the same MU discharge pattern, only delayed of a few samples. This is done by computing the cross-correlation between all the detected trains: if two or more trains exceeds a similarity threshold, only the train resulted from the more homogeneous cluster is mantained.

6. Given the discharge timings and the original data, recover the MUAP time-courses through spike-triggered averaging.

Simulation Results

The algorithm was tested in different situations with a variable number of MUAPs, depending on the force level.

The evaluation of the decomposition is not an easy task in case of experimental EMG data. Intramuscular recordings able to isolate single MUAPs are needed, even if also their reliability should be validated. Conversely, in the case of simulated data, the ground truth was available, thus the performances of the algorithm could be evaluated precisely. It has to be said, however, that the simulations are only a model of reality (for example, they do not take account of the possible change of shape of the MUAP waveforms during time), so the reliability of the decomposition algorithm on experimental data should be further investigated.

The number of correctly recovered MUAPs was evaluated by computing a normalized maximum of the cross-correlation between the reconstructed and the original trains:

$$XC_{i,j} = \frac{2 * max\big(\int \hat{s}_i(t) s_j(t+\tau)\big)}{\sum_{k=1}^{T} \hat{s}_i(k) + \sum_{w=1}^{T} s_j(w)} \tag{3.11}$$

where s_i are the simulated firing trains and $\hat{s_j}$ are the reconstructed ones. The values of XC ranges from 0 to 1, the latter indicating perfect reconstruction. For all the reconstructed trains with $XC > 0.9$, the timecourses of the MUAPs on the electrodes were recovered with a spike triggered averaging. A 2-D correlation coefficient (CC) was then computed between the original MUAP timecourses and the reconstructed ones on all the 63 channels in order to have an overall index of the goodness of the reconstruction for every single MUAP.

The reconstructed trains on all the channels were then summed to obtain the reconstructed interference signal, that was used to evaluate the overall decomposition yield:

$$DY(\%) = 100 - 100 * \frac{RMS(\mathbf{x} - \hat{\mathbf{x}})}{RMS(\mathbf{x})} \tag{3.12}$$

where $\mathbf{x}$ is the original matrix containing the EMG signal and $\hat{\mathbf{x}}$ is the reconstructed one, obtained as the sum of all the reconstructed MUAPs. RMS is the root mean square, that is a useful parameter to determine the strength of contraction of a muscle from the sEMG and is dependent from the number and from the size of the MUAPs.

In order to provide a simple example of decomposition, two simulations were carried out with respectively 5 and 10 MUAPs with a matrix of 32 channels and an extension factor $K = 2$. Since the resulting signals were very simple, a spatially white Gaussian noise (that is a reasonable approximation of EMG noise) with signal to noise ratio (SNR) of 30 dB was also added to the observations. In the first case,

all the three ICA algorithms correctly reconstructed the 5 MUAPs, with a mean decomposition yield of 68,76%. In the second simulation, the dectected MUAPs were 4 for robustICA and infomax and 5 for fastICA, with a mean decomposition yield of 55,1%, indicating that as the number of motor units increases, the algorithm has some limitation in detecting the MUAPs with lower frequency or with a smaller waveform, as can be seen in Figure 3.6, where a 1-second portion of the original and reconstructed signals on channel 10 is shown as example. Moreover, the ICA approach highly suffers the presence of Gaussian sources, so the presence of the noise on each channel, even of small amplitude, causes a loss of performances of the ICA algorithms. The EMG decomposition on real data with ICA is then performed with the assumption that not too many Gaussian sources are present.

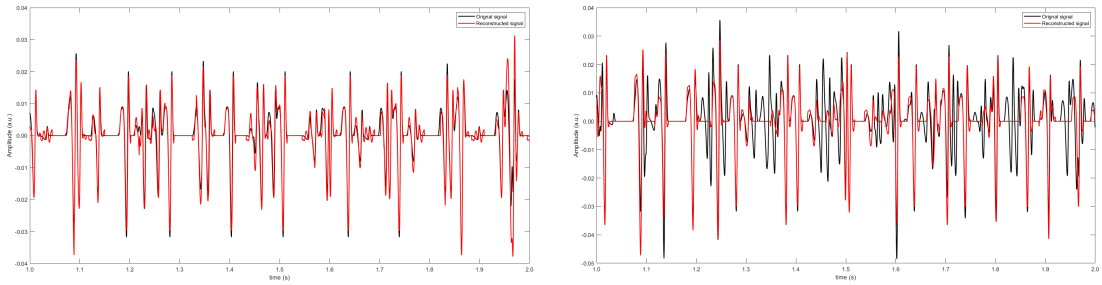

Figure 3.6: *Example of a portion of simulated and reconstructed signals on channel* 10. *On the left, a simulation with* 5 *MUAPs and a mean decomposition yield of* 68,76%, *on the right a simulation with* 10 *MUAPs and a mean decomposition yield of* 55,1%.

In order to test the performances in a more realistic condition, three different levels of force were considered: $3\%, 20\%$ and 50% MVC, with a number of MUAPs ranging from 80 (3% MVC) to 286 (50% MVC). Moreover, with the increase of the force level, the frequency of the discharge timings of the MUAPs highly increased. Five simulations were performed for each force level and for each of the three ICA algorithms. The results are showed in Figure 3.7 and Figure 3.8. The number of correctly reconstructed sources, the correlation coefficient obtained by comparing them with the simulated trains and the decomposition yield are showed; on the top right of each panel, a portion of the timecourse from electrode 10 with the superimposed reconstructed signal is also reported.

As said before, with the increase of the force level, the spikes highly increased with it: expecially at high levels of force, the new recruited motor units have high discharge frequency. Moreover, the interference signal becomes highly complex and the problem, having only 63 available observations, becomes more and more underdetermined. As can be seen, the performances of the algorithm were very affected fom this fact. Note that the extension with the $K - 1$ delayed replicas does not seems to help in this sense, since with the replicas also the independent

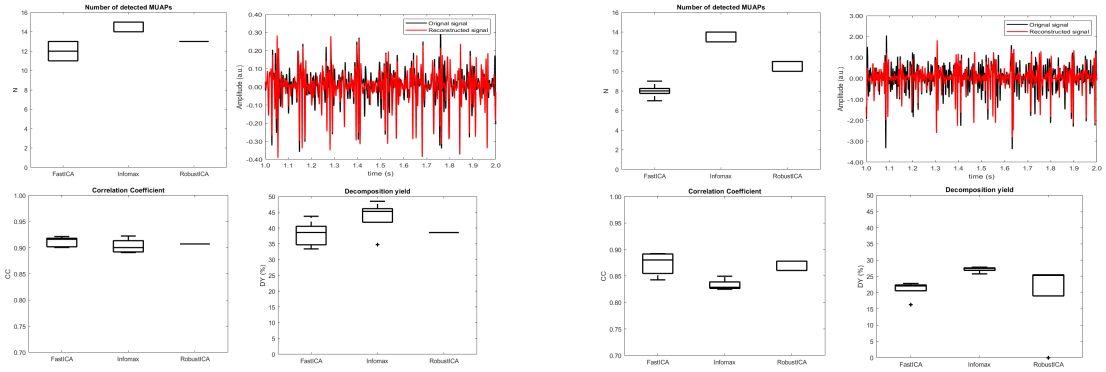

Figure 3.7: *Simulations with* 3% *MVC (left) and* 20% *MVC (right). The number of correctly reconstructed MUAPs, the correlation coefficient, the overall yield of decomposition and a portion of simulated and reconstructed signals are showed.*

sources increased with a factor $K - 1$. The extension factor can then be seen as a trick to obtain an higher number of independent components and then to increase the probability to detect an higher number of different MUAPs. Moreover, it allows to keep the assumptions of ICA valid in case of small delay between the sources in different channels (for example due to propagation if the electrode array is parallely oriented to the muscle fibers). In fact, without the extension factor, a source contribution with a small delay on a channel with respect to the same source contribution on another channel would be treated as an independent source.

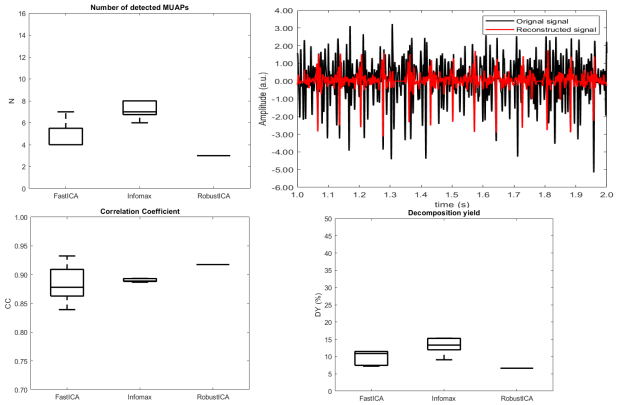

Figure 3.8: *Simulation with* 50% *MVC. The number of correctly reconstructed MUAPs, the correlation coefficient, the overall yield of decomposition and a portion of simulated and reconstructed signals are showed.*

It is important to stress that a complete decomposition recovering all the MUAPs cannot be reached, even with small levels of force. In the literature one can find that state of the art methods can detect no more then 50% of the MUAPs [6], with a number of simulated trains equal to 86 (that are similar to the previous simulated force level 3%) and with higher extension factors, that requires higher computational power and increased time for the decomposition. Moreover, if the threshold of similarity between the reconstructed and the simulated trains is lowered, more

MUAPs can be considered as correctly reconstructed, even if they possess only a partial match with the simulated ones.

By comparing the three ICA algorithms, infomax seems to reach the best results, with the higher number of reconstructed MUAPs and a good decomposition yield. However, the reconstruction is less accurate for infomax (as can be seen from the lower correlation coefficient), while robustICA provides high accuracy in the reconstructed trains and mantains the more stable results in all the simulations. With high levels of force, the MUAP trains have very different numbers of spikes, so the method has some limitations due to the k-means clustering, that needs to know in advance an approximate value for the number of discharge events in order to compute the number of clusters. Different methods to discriminate between the spikes of the independent components can be further investigated, in order to obtain good performances even if the trains have very different number of discharge timings.

Chapter 4

An Alternative Method for Crosstalk Reduction

4.1 The Problem of Crosstalk

Crosstalk is still an open problem in the EMG acquisition. As discussed in the previous chapter, it limits the applications of surface EMG and it is impossible to remove with simple linear filtering, as also part of the signal of interest would be removed. Moreover, it is also difficult to assess and evaluate its contribution, as the crosstalk signal can assume a different waveform with respect to the signal recorded on the muscle that produces it because of the propagating medium and of the position of the electrodes. This makes unreliable the crosstalk quantification by using the correlation between the signals, that would be the more simple and intuitive way to evaluate its contribution. In fact, an higher value could mean only a correlation in motor units discharge pattern in adjacent muscles, rather then a common electrical source [15]. This means that also co-activation of adjacent muscles can be erroneously confused with crosstalk.

The techniques discussed in the previous, such as the SOBI method, are based on assumptions that are not always valid in experimental conditions: for example, the mixing matrix could change during the recording, so it should be calculated many times for each new portion of data. This limits real-time applications of BSS techniques, as they are usually computational expensive.

The method proposed in the following is based on an adaptive filter, that fits to the anatomical and experimental conditions (e.g. conductivity of the tissues, position and type of the electrodes) and is stable and suitable for real-time applications. It mantains the energy of the muscle of interest, by reducing that from other sources, by filtering both in time and among the channels [17].

4.2 Optimal Spatio-Temporal Filter

An Optimal Spatial Filter (OSF) can be designed with a linear combination of the data from different channels weighted by the coefficients w_i, such that it maximizes the signal to crosstalk ratio (SCR):

$$SCR = 10log_{10}\frac{\left\|\sum_{i=1}^{M} w_i S_i(t)\right\|^2}{\left\|\sum_{i=1}^{M} w_i C_i(t)\right\|^2} \tag{4.1}$$

where $S_i(t)$ is the portion of signal from the muscle of interest in the i^{th} channel at time t and $C_i(t)$ is the crosstalk contribution. The log-function can be maximized by maximizing its argument, that can be rewritten as:

$$J(w) = \frac{\left\|\sum_{i=1}^{M} w_i S_i(t)\right\|^2}{\left\|\sum_{i=1}^{M} w_i C_i(t)\right\|^2} = \frac{w^T \mathbf{S^T S} w}{w^T \mathbf{C^T C} w} = \frac{w^T \mathbf{R_S} w}{w^T \mathbf{R_C} w} \tag{4.2}$$

where $\mathbf{R_S}$ and $\mathbf{R_C}$ are the autocorrelation matrices of the signal and of the crosstalk.

The optimization problem can be solved by maximizing the numerator, such that $w^T \mathbf{R_C} w$ equals 1. The study of the Lagrangian:

$$L_P = \frac{1}{2} w^T \mathbf{R_S} w + \frac{1}{2}\lambda(1 - w^T \mathbf{R_C} w) \tag{4.3}$$

brings to the following equation, that is an eigenvalue problem:

$$\mathbf{R_S} w = \lambda \mathbf{R_C} w \quad \longrightarrow \quad \mathbf{R_C^{-1} R_S} w = \lambda w \tag{4.4}$$

However, the matrix $\mathbf{R_C^{-1} R_S}$ is not symmetric, but a change of variable and the introduction of the vector $v = \mathbf{R_S^{1/2}} w$ brings to:

$$\mathbf{R_S^{1/2} R_C^{-1} R_S^{1/2}} v = \lambda v \tag{4.5}$$

The eigenvalues λ_k are then positive and the eigenvectors v_k are orthogonal. Therefore, the maximization of the SCR is performed with the detection of the largest

eigenvalues, as the associated eigenvectors correspond to the optimal weights for the filter.

The OSF can be generalized by considering also past values of the EMG: this brings to the Optimal Spatio-Temporal Filter (OSTF), that selects the weights of a linear combination of present and past values from different channels in order to maximize the SCR. This is done by including the correlation matrices of the delayed data in the eigenvalue problem of Equation 4.5. The optimal weights can then be selected by providing to the filter a portion of data (the training set) containing selective activations of the muscles.

The OSTF has two parameters that can be changed: the delay τ between subsequent samples and the order of the temporal filter. This can be done, for example, by evaluating the performances on a validation set, in order to select the best parameters and avoid overfitting on the training data.

4.2.1 Experimental Signals

The signals were acquired at LISiN, Politecnico di Torino, with the MEACS system, by using two linear adhesive electrode arrays. Each array had 32 channels and was connected to a sensor unit that performed conditioning, sampling and wireless transmission of the 32 monopolar signals. The sample frequency was 2048 Hz.

One array was placed on the Tibialis Anterior (TA), the other on Peroneus Longus (PL), that are two antagonist muscles of the lower leg. The TA is involved in dorsiflexion and inversion of the foot, while PL participates in the plantarflexion and eversion. Figure 4.1 shows the electrode placement and summarizes the movements performed by TA and PL.

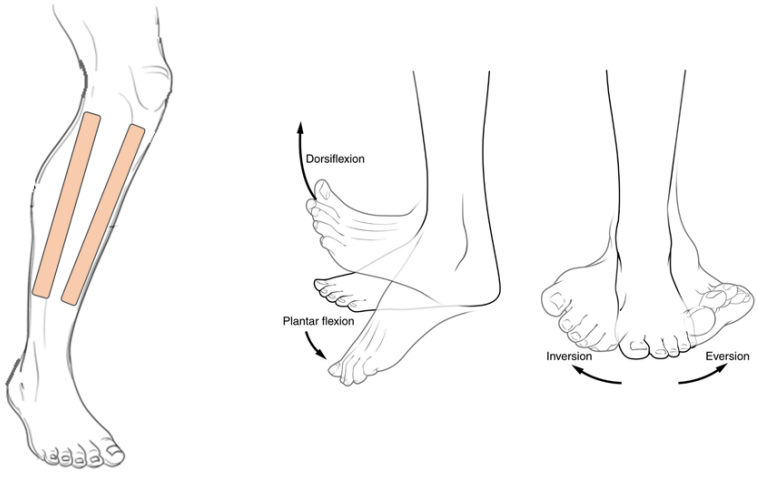

Figure 4.1: *Position of the two electrode arrays (left) and movements in which TA and PL are involved (right).*

The protocol consisted in the selective activation of the two muscles, by performing isometric dorsiflexions and eversions at three different levels of force. For each muscle, four trials were performed, with a low, medium and high level of force. By recording the signal on the muscle that was not active, the crosstalk contribute was evident, as no signal was expected on that channels. An example of a portion of the recorded signals during the dorsiflexion task is showed in Figure 4.2, where TA is active and propagation of the potentials starting from the innervation zone (IZ) can be appreciated. PL is expected to be inactive in this situation. However, small amplitude signals are visible also on this muscle: they don't show a clear direction of propagation and are expected to be crosstalk from the TA. Note that, in order to make clearer the visualization, the signals were normalized with the maximum value of each muscle: the signals detected on PL are an order of magnitude smaller than those detected on TA, as can be seen from the normalization value.

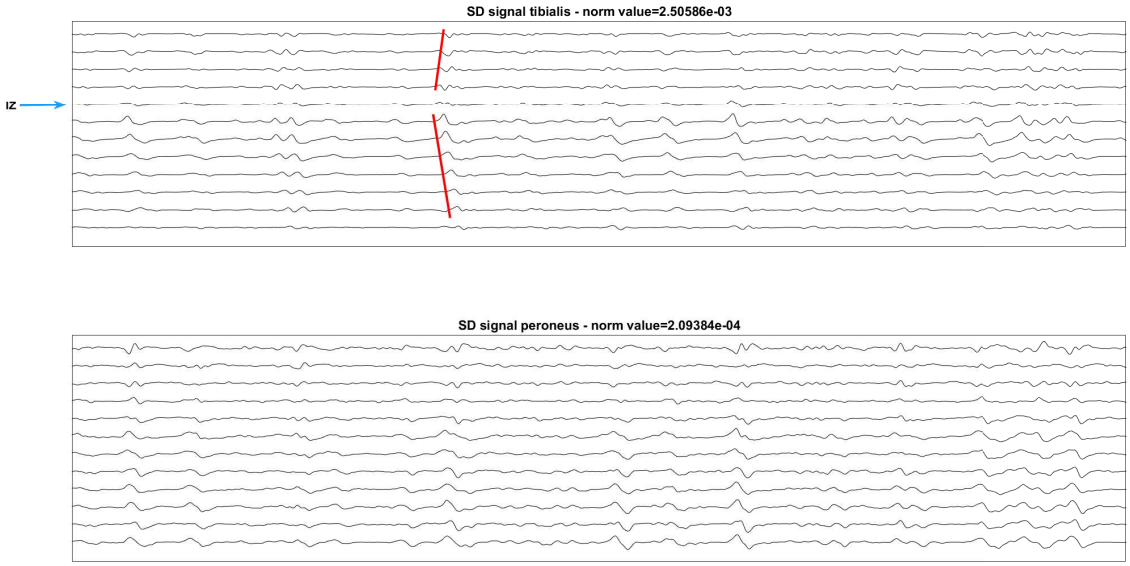

Figure 4.2: *Portion of signals recorded on TA and PL during a dorsiflexion task. The innervation zone and the directions of propagation are showed on the signals from TA.*

Results

In order to evaluate the performances of the filter, two of the trials were used as training set, while the other two were used as test set. The training set was build by concatenating alternative activations of the two muscles, recorded on different monopolar channels placed both on TA and PL. In this first part, TA was considered as the muscle of interest, while PL was the source of crosstalk. The signals were selected from 6 channels: 3 of them were located on TA, the other 3 on PL. The

selection of the channels for the training set is a critical point, as it influences the weights of the filter and the subsequent results: after a visual analysis, channels from 27 to 29 on both the arrays were chosen, as the signals mantained a similar shape and propagation was evident for TA. The best results on the training set were obtained with a length of the temporal filter equal to 8 and with a delay between consequent samples equal to 2: these parameters were then kept fixed in the following. The obtained weights were applied to the test set: it was composed by simulating a simultaneous activation of the two muscles. The signals recorded on TA during the PL activation (i.e. the crosstalk) were summed to the epochs of TA activations. The same thing was done on PL, where the TA contribute recorded on it during dorsiflexions was summed. Thus, the test set is similar to the training set, but the activations are not yet selective, as they overlap in time: infact, the length of the test set is the half of that of the training set. The obtained signals are showed in Figure 4.3.

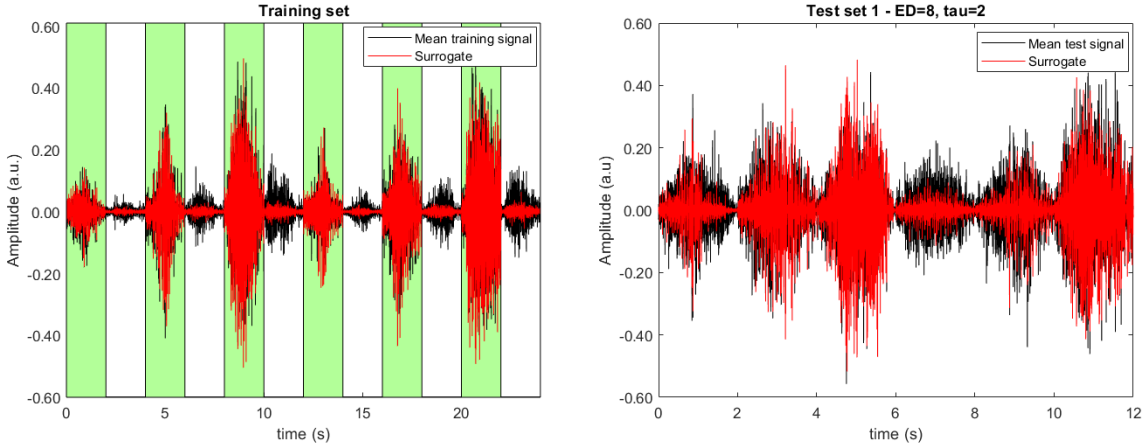

Figure 4.3: *Mean training signal on the channels placed on TA with superimposed surrogate (left). Mean test signal with superimposed surrogate (right).*

On the left, the mean training signal on the channels placed on TA with the superimposed surrogate is showed. The epochs containing TA activations are highlighted in green. The other epochs correspond to crosstalk, as they contain signals recorded on TA during PL activations. On these epochs, the reduction of the crosstalk contribution when computing the surrogate channel is evident. On the right, the mean test signal with the superimposed surrogate is reported: the crosstalk reduction is particularly evident for low levels of force.

A second test set was created in the same way as the first showed before, but moving of one channel towards the innervation zone: thus, channels from 26 to 28 on both muscles were considered. The filter was applied with the same weights to this second test set. The obtained surrogates from the two test sets were then used to compute the conduction velocity (CV) of the muscle fibers, by using a

maximum likelihood estimator [10] and by dividing the signals in epochs of 500 ms. SD channels obtained from the monopolars used to build the surrogates were used as reference. The CV was also computed on the test sets with crosstalk and on two surrogates obtained by applying the filter to two new test sets, built with the same electrodes of the first but with no crosstalk contribution summed on them. The error between the couples of estimates was evaluated as:

$$ERR = \frac{std(CV_1 - CV_2)}{std(CV_1)} \tag{4.6}$$

where CV_1 were the CV values computed on the epochs of respectively the original SDs and the surrogates and CV_2 were the values of CV of the epochs of the test sets corrupted by crosstalk and of the surrogates obtained by the test sets without the crosstalk. As expected, the error on the surrogate channels was on average lower then that on the SD channels. This means that the OSTF correctly removed the crosstalk, by leaving the signals almost unchanged when this was not present. The crosstalk highly biased the CV estimates on the SD channels, giving rise to unstable results. The errors on the CV estimation are summarized in Table 4.1, for different numbers of channels used to train the filter (and then to build the surrogates). For each number of channels, the three values correspond to a low, medium and high level of summed crosstalk.

Number of channels	**Single differentials**	**Surrogate channels**
4	0,2364	0,2918
	0,4743	0,3763
	0,3290	0,2810
6	0,3782	0,2142
	0,4324	0,2043
	0,6544	0,2902
8	0,2789	0,2965
	0,4170	0,2523
	0,5526	0,2930

Table 4.1: *CV errors on TA for different numbers of channels used for the OSTF and for low, medium and high levels of summed crosstalk.*

The best results were obtained with 6 channels: even if the information given to the OSTF is less than that provided with 8 channels, the shapes of the waveforms were more homogeneous and the surrogate channels obtained were probably more accurate. Note that the CV estimate with SD channels outperformed the surrogate

estimate in only two cases. They both correspond to a low level of crosstalk: this means that the difference between the original SD channels and the test signals with added crosstalk was very low and this brought to a lower bias in the CV estimates. Moreover, the OSTF was more prone to overfitting in this situation, as the training data contained higher levels of crosstalk with respect to the test data.

Regarding the peroneus, the eversion tasks turned out to be not selective: a clear activation of TA could be seen from the signals recorded on this muscle. This reflected also in a high bias in computing the conduction velocity due to the crosstalk contribution on PL. In this situation, 3 single differential channels (obtained offline from the recorded monopolars) were selected on each muscle for the training of the OSTF. The obtained surrogates and the original SDs used to generate them were then used to compute the CV, by using epochs of 500 ms. The CV was also computed for the SD channels corrupted by crosstalk and for the surrogates generated with noise free data, in the same way used for the dorsiflexion task explained before. Figure 4.4 shows the results of CV estimates for the different epochs, with the summation of a high level of crosstalk. Note the higher values for both the noise free and the SD channels with summed crosstalk, that are out of the physiological range. By using the surrogate channels, however, the values seem to be more reasonable. The reduced error between the couples of CV estimates suggests that the summed crosstalk contribution (for all the three levels) recorded during the dorsiflexion has not great effect: the OSTF seems to reduce the crosstalk that was already present on the signals, by making more feasible the CV estimation. Infact, the filter was trained with the signals recorded on TA during activation, so it learned to reduce them. This is in line with [17], where the OSTF gave good results in simulation also with a training set made with few not selective activations of the muscle of interest.

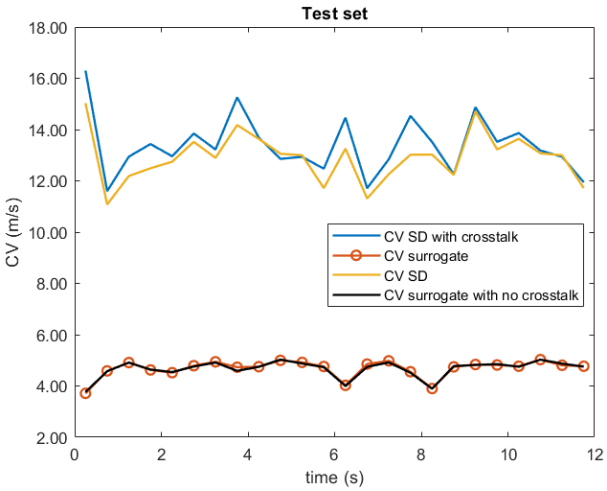

Figure 4.4: *CV estimates on PL for the original SD channels with and without a summed high level of crosstalk and for the surrogates obtained from them.*

APPENDIX

Eigendecomposition

The eigendecomposition is the factorization of a matrix $\mathbf{A}$ in its eigenvalues and eigenvectors:

$$\mathbf{Av} = \mathbf{Dv} \tag{A.1}$$

where $\mathbf{v}$ contains the eigenvectors of $\mathbf{A}$ on the columns and $\mathbf{D}$ is a diagonal matrix containing the eigenvalues λ_i. The equation in the eigenvalues then becomes:

$$(\lambda\mathbf{I} - \mathbf{A})\mathbf{v} = 0 \tag{A.2}$$

Since $\mathbf{v}$ is non-zero, the eigenvalues can be obtained by computing $\det(\lambda\mathbf{I} - \mathbf{A})$.

Note that, in order to perform this decomposition, the matrix $\mathbf{A}$ must be diagonalizable, i.e. it has to be squared.

Singular Value Decomposition

If the matrix $\mathbf{A}$ is not a square matrix, eigendecomposition cannot be performed. However, it can be factorized with singular value decomposition (SVD), that can be considered as a generalization of eigendecomposition:

$$\mathbf{A} = \mathbf{U\Sigma V^T} \tag{A.3}$$

where $\mathbf{A}$ is a $M \times N$ matrix, $\mathbf{U}$ and $\mathbf{V}$ are respectively $M \times M$ and $N \times N$ unitary matrices and $\mathbf{\Sigma}$ is a diagonal matrix that contains the singular values σ_i in descending order. Note that the singular values are the square roots of the eigenvalues of the square matrices $\mathbf{AA^T}$ and $\mathbf{A^TA}$, while unitary means that $\mathbf{UU^T} = \mathbf{I}$ and $\mathbf{VV^T} = \mathbf{I}$.

The vectors $\vec{u_i}$ and $\vec{v_i}$ are the eigenvectors of $\mathbf{AA^T}$ and $\mathbf{A^TA}$, respectively. They are placed on the columns of $\mathbf{U}$ and $\mathbf{V}$ and are called singular vectors.

Spatial Whitening

Spatial whitening is a procedure to transform the data such that it has an identity covariance matrix, i.e. the dimensions are uncorrelated and the variance along each dimension equals to 1.

By considering the covariance matrix:

$$\mathbf{C} = Cov(\mathbf{X}) = E[\mathbf{XX^T}] = \frac{\mathbf{XX^T}}{n} \tag{A.4}$$

that is symmetric and positive semi-definite, it can be decomposed with eigenvalues and eigenvectors:

$$\mathbf{C} = \mathbf{EDE^{-1}} \tag{A.5}$$

where $\mathbf{D}$ is a diagonal matrix containing the eigenvalues on the diagonal and $\mathbf{E}$ is the matrix of eigenvectors.

Then, by rearranging (A.5), the covariance matrix can be transformed into the diagonal matrix $\mathbf{D}$:

$$\mathbf{E^{-1}CE} = \mathbf{D} \tag{A.6}$$

Given a matrix $\mathbf{X}$, the goal is then to find a matrix $\mathbf{W_D}$ such that:

$$\mathbf{Y} = \mathbf{W_D X} \tag{A.7}$$

where $\mathbf{Y}$ has a diagonal covariance $\mathbf{D}$:

$$\mathbf{D} = Cov(\mathbf{Y}) = \frac{\mathbf{W_D X}(\mathbf{W_D X})^T}{n} = \mathbf{W_D W_D^T C} \tag{A.8}$$

then, from Equation (A.6), we obtain:

$$\mathbf{E^{-1}CE} = \mathbf{W_D W_D^T C} \tag{A.9}$$

by premultiplying by $\mathbf{C^{-1}}$ and since $\mathbf{E^{-1}} = \mathbf{E^T}$:

$$\mathbf{E^T E} = \mathbf{W_D W_D^T} \tag{A.10}$$

then, $\mathbf{W_D} = \mathbf{E^T}$, that is the transpose of the matrix of eigenvectors of the covariance matrix.

Now the data is uncorrelated. But also a unitary variance is desired such that $\mathbf{D^{-1}D} = \mathbf{I}$, that can be written as:

$$\mathbf{D^{-1}} = \mathbf{D^{-1/2}ID^{-1/2}} \tag{A.11}$$

then, by using (A.6), we found the matrix $\mathbf{W_W}$ that brings to an identity covariance matrix:

$$\mathbf{W_W} = \mathbf{D^{-1/2}E^T} \tag{A.12}$$

Note that the whitening procedure can be performed also with SVD, by using singular values and singular vectors in place of eigenvalues and eigenvectors.

Pseudoinversion

The inverse of a matrix $\mathbf{A}$ is defined as:

$$\mathbf{A^{-1}} = \frac{1}{det(\mathbf{A})} adj(\mathbf{A}) \tag{A.13}$$

where $adj(\mathbf{A})$ is the adjoint of $\mathbf{A}$. In order to perform the inversion, the matrix must be squared and must have non-zero determinant: otherwise pseudoinversion, that can be considered as a generalization of inversion, is needed.

The pseudoinverse of $\mathbf{A}$ can be obtained from its SVD:

$$\mathbf{A}^{\#} = \mathbf{V\Sigma^{-1}U^T} \tag{A.14}$$

Note that, given a linear system $\mathbf{Ax} = b$ with $\mathbf{A}$ being a not-squared matrix, the solution can be obtained by minimizing:

$$\mathbf{y} = \min_x \|\mathbf{Ax} - b\|^2 \tag{A.15}$$

then, by premultiplying by $\mathbf{A^T}$ and being $\mathbf{y}$ orthogonal to $Im(\mathbf{A})$, the solution can be recovered:

$$\mathbf{A^T y} = \mathbf{A^T}(\mathbf{Ax} - b) = 0 \tag{A.16}$$

$$\mathbf{A^T Ax} = \mathbf{A^T} b$$

$$\mathbf{x} = (\mathbf{A^T A})^{-1}\mathbf{A^T} b \tag{A.17}$$

where $(\mathbf{A^T A})^{-1}\mathbf{A^T}$ is the pseudoinverse of $\mathbf{A}$.

References

[1] Anthony J Bell and Terrence J Sejnowski. An information-maximization approach to blind separation and blind deconvolution. *Neural computation*, 7(6):1129–1159, 1995.

[2] Adel Belouchrani, Karim Abed-Meraim, J-F Cardoso, and Eric Moulines. A blind source separation technique using second-order statistics. *IEEE Transactions on signal processing*, 45(2):434–444, 1997.

[3] Adel Belouchrani and Moeness G Amin. Blind source separation based on time-frequency signal representations. *IEEE Transactions on Signal Processing*, 46(11):2888–2897, 1998.

[4] Sergio Cruces-Alvarez, Andrzej Cichocki, and Luis Castedo-Ribas. An iterative inversion approach to blind source separation. *IEEE Transactions on Neural Networks*, 11(6):1423–1437, 2000.

[5] Chenyun Dai and Xiaogang Hu. Independent component analysis based algorithms for high-density electromyogram decomposition: Experimental evaluation of upper extremity muscles. *Computers in Biology and Medicine*, 2019.

[6] Chenyun Dai and Xiaogang Hu. Independent component analysis based algorithms for high-density electromyogram decomposition: Systematic evaluation through simulation. *Computers in biology and medicine*, 109:171–181, 2019.

[7] Anders M Dale, Arthur K Liu, Bruce R Fischl, Randy L Buckner, John W Belliveau, Jeffrey D Lewine, and Eric Halgren. Dynamic statistical parametric mapping: combining fmri and meg for high-resolution imaging of cortical activity. *Neuron*, 26(1):55–67, 2000.

[8] Arnaud Delorme and Scott Makeig. Eeglab: an open source toolbox for analysis of single-trial eeg dynamics including independent component analysis. *Journal of neuroscience methods*, 134(1):9–21, 2004.

[9] Arnaud Delorme, Jason Palmer, Julie Onton, Robert Oostenveld, and Scott Makeig. Independent eeg sources are dipolar. *PloS one*, 7(2):e30135, 2012.

[10] Daniela Farina, Wrya Muhammad, Elena Fortunato, Olivier Meste, Roberto Merletti, and Hervé Rix. Estimation of single motor unit conduction velocity from surface electromyogram signals detected with linear electrode arrays. *Medical and Biological Engineering and Computing*, 39(2):225–236, 2001.

[11] Dario Farina, Cédric Févotte, Christian Doncarli, and Roberto Merletti. Blind

separation of linear instantaneous mixtures of nonstationary surface myoelectric signals. *IEEE Transactions on Biomedical Engineering*, 51(9):1555–1567, 2004.

[12] Roberta Grech, Tracey Cassar, Joseph Muscat, Kenneth P Camilleri, Simon G Fabri, Michalis Zervakis, Petros Xanthopoulos, Vangelis Sakkalis, and Bart Vanrumste. Review on solving the inverse problem in eeg source analysis. *Journal of neuroengineering and rehabilitation*, 5(1):25, 2008.

[13] Ales Holobar and Damjan Zazula. Multichannel blind source separation using convolution kernel compensation. *IEEE Transactions on Signal Processing*, 55(9):4487–4496, 2007.

[14] Aapo Hyvärinen and Erkki Oja. Independent component analysis: algorithms and applications. *Neural networks*, 13(4-5):411–430, 2000.

[15] Madeleine M Lowery, Nikolay S Stoykov, and Todd A Kuiken. A simulation study to examine the use of cross-correlation as an estimate of surface emg cross talk. *Journal of Applied Physiology*, 94(4):1324–1334, 2003.

[16] Ali Mansour, Nabih Benchekroun, and Cedric Gervaise. Blind separation of underwater acoustic signals. In *International Conference on Independent Component Analysis and Signal Separation*, pages 181–188. Springer, 2006.

[17] Luca Mesin. Optimal spatio-temporal filter for the reduction of crosstalk in surface electromyogram. *Journal of neural engineering*, 15(1):016013, 2018.

[18] Danielle Nuzillard and Albert Bijaoui. Blind source separation and analysis of multispectral astronomical images. *Astronomy and Astrophysics Supplement Series*, 147(1):129–138, 2000.

[19] Kenneth J Pope and Robert E Bogner. Blind signal separation i. linear, instantaneous combinations: I. linear, instantaneous combinations. *Digital Signal Processing*, 6(1):5–16, 1996.

[20] Mikhail Rozhkov and Ivan Kitov. Blind source separation of seismic events with independent component analysis: Ctbt related exercise. *EGU*, (5496), 2015.

[21] Michael Scherg. Fundamentals of dipole source potential analysis. *Auditory evoked magnetic fields and electric potentials. Advances in audiology*, 6:40–69, 1990.

[22] Michael Pedersen Syskind, Jan Larsen, Ulrik Kjems, and Lucas C Parra. A survey of convolutive blind source separation methods. *Springer Handbook on Speech Processing and Speech Communication*, 2007.

[23] Jose Antonio Urigüen and Begoña Garcia-Zapirain. Eeg artifact removal—state-of-the-art and guidelines. *Journal of neural engineering*, 12(3):031001, 2015.

[24] V Zarzoso, AK Nandi, and E Bacharakis. Maternal and foetal ecg separation using blind source separation methods. *Mathematical Medicine and Biology: A Journal of the IMA*, 14(3):207–225, 1997.

[25] Vicente Zarzoso and Pierre Comon. Robust independent component analysis

by iterative maximization of the kurtosis contrast with algebraic optimal step size. *IEEE Transactions on neural networks*, 21(2):248–261, 2009.

[26] Leonid Zhukov, David Weinstein, and Chris Johnson. Independent component analysis for eeg source localization. *IEEE Engineering in Medicine and Biology Magazine*, 19(3):87–96, 2000.